DYNAMIC SIMULATION OF DUAL GRADIENT DRILLING OPERATION USING THE FINITE ELEMENT METHOD

A Thesis

by

FIDEL FERNANDES PEREIRA

Submitted to the Office of Graduate and Professional Studies of
Texas A&M University
in partial fulfillment of the requirements for the degree of

MASTER OF SCIENCE

Chair of Committee,	Jerome J. Schubert
Committee Members,	Samuel F. Noynaert
	Joseph E. Pasciak
Head of Department,	A. Daniel Hill

August 2016

Major Subject: Petroleum Engineering

Copyright 2016 Fidel Fernandes Pereira

ABSTRACT

The deepwater and ultra-deepwater drilling industry has created several techniques to overcome the Well-Control challenge in these scenarios. Dual Gradient Drilling is one of those techniques.

Created in the mid-90's the technique is relatively new and it is not fully integrated at the market yet. The main concept it is to use a lighter fluid on top of a heavier fluid inside the wellbore and marine riser, which allows the engineer a better control of bottomhole pressure.

This work is focused on understand the fluid dynamics of a Dual Gradient Drilling operation. It uses the conservation equation along with the previous proposed density and rheological model to investigate how mud weight, thermal properties and well configuration affect the pressure and temperature profile. The system of equation is discretized using Finite Element Methods and the code implemented in Matlab®.

The results demonstrated the importance of an accurate density model and its consideration during the development of the well plan. A sensitivity analysis shows the effects of the Overall Heat Transfer Coefficient over the temperature profile, proving that it is the major parameter controlling the heat exchange in the drilling process.

DEDICATION

To my mother and family.

ACKNOWLEDGEMENTS

I would like to thank my committee chair, Dr. Schubert, and my committee members, Dr. Noynaert and Dr. Pasciak for their support throughout the course of this research.

Thanks also go to my friends and colleagues and the department faculty and staff for making my time at Texas A&M University a great experience. I also want to extend my gratitude CAPES Foundation and the Ministry of Education of Brazil for the financial support through the scholarship process 88888.075990/2013-00.

Finally, thanks to my mother and family for their patience and love and to my friends from Brazil for their encouragement.

TABLE OF CONTENTS

LIST OF FIGURES

Page

LIST OF TABLES

Page

1 INTRODUCTION

The oil industry is well known for its successful history of overcoming challenges. It is continuously searching for the new reserves and developing new technologies to explore what was once considered unexplored. These new reserves usually are located in challenging environments, such as offshore oilfields in ultra-deep waters.

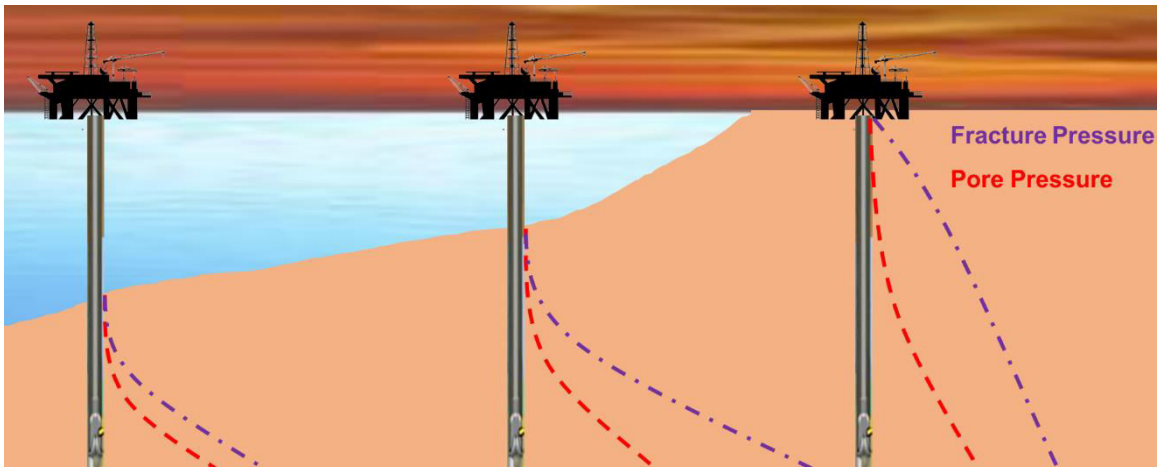

Figure 1.1 – Illustration of the Operational Window in Different Water Depth.

One of the most challenging problems in deepwater drilling is the narrowing of the Operational Window – the range between pore pressure and fracture pressure – as

the water depth increases. Figure 1.1 illustrates this fact, for three different wells with the same target depth, but different water depth, the layer of sediment above target depth reduces as the water depth increases, creating a greater water overburden. Besides that, the project faces feasibility issues, such as needing longer and heavier risers, consequently bigger and more expensive drilling rigs.

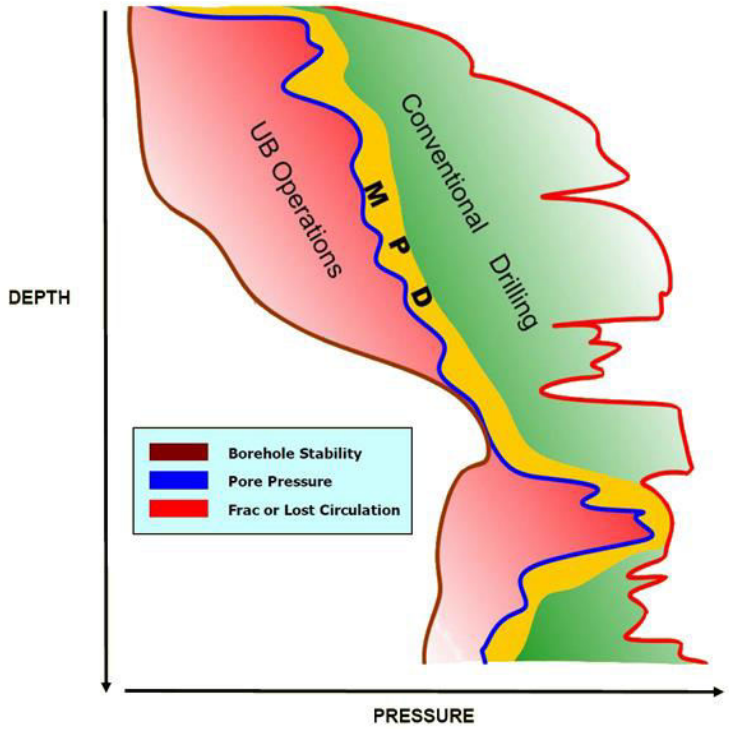

Figure 1.2 - Drilling Window Showing the Different Drilling Techniques Approach. (after Malloy et al., 2009)

In order to overcome these issues, the management of the annular Bore Hole Pressure (BHP) must be carefully planned prior of each drilling section, in order to avoid Non-Productive Times (NPT). This can be achieved by Conventional Drilling, Underbalanced Operations (UBO) or Managed Pressure Drilling (MPD). Figure 1.2 illustrates the general domain of these different drilling techniques.

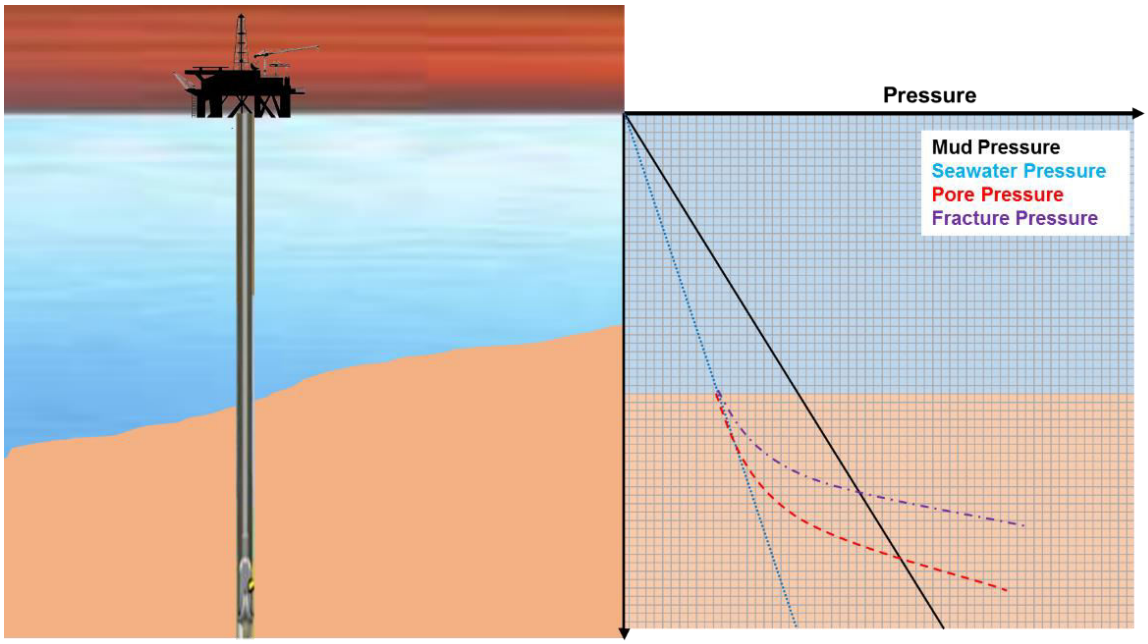

Figure 1.3 – Conventional Drilling Pressure Profile.

In Conventional Drilling, pressure is managed by single mud density running inside of the drilling string, wellbore and marine riser, which creates a constant pressure

gradient, Figure 1.3, but as water depth increases, this technique becomes unpractical, because a change in the BHP means a change in the mud density of the whole well.

Managed Pressure Drilling is defined in the glossary of IADC (2011), Committee of UBO and MPD, as "an adaptive drilling process used to more precisely control the annular pressure profile throughout the wellbore. The objectives are to ascertain the downhole pressure environment limits and to manage the annular hydraulic pressure profile accordingly. This may include control of back pressure, fluid density, fluid rheology, annular friction pressure level, circulating friction, and hole geometry or combinations thereof".

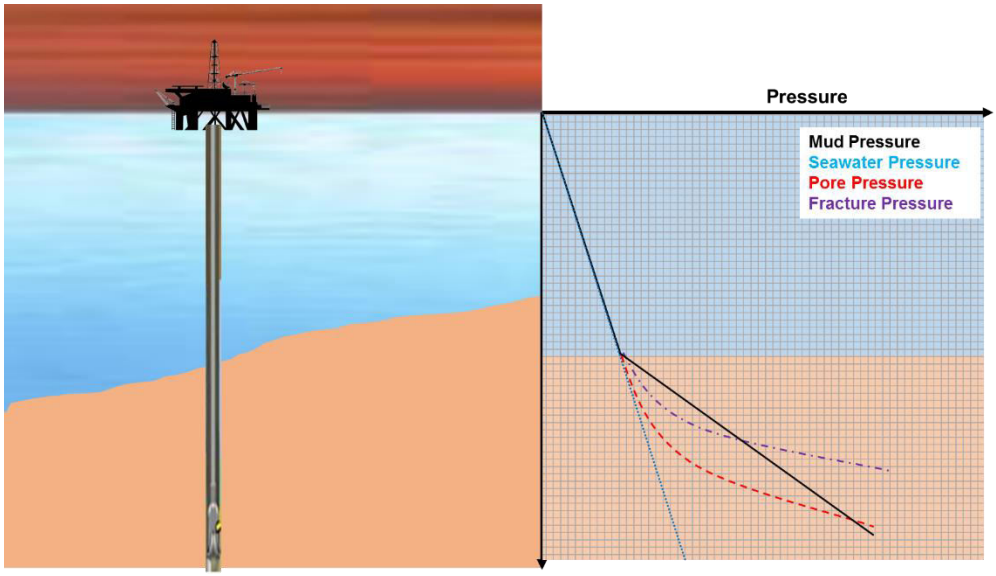

Figure 1.4 – Managed Pressure Drilling Pressure Profile.

Different techniques are available in the industry. Each one focused on controlling pressure through one of the parameters listed above. The Dual Gradient Drilling is a techniques focused on the management of the density of one or more fluids inside the wellbore and marine riser. Figure 1.4 illustrates the technique in which a lighter fluid is on top of a heavier mud, creating a dual pressure gradient.

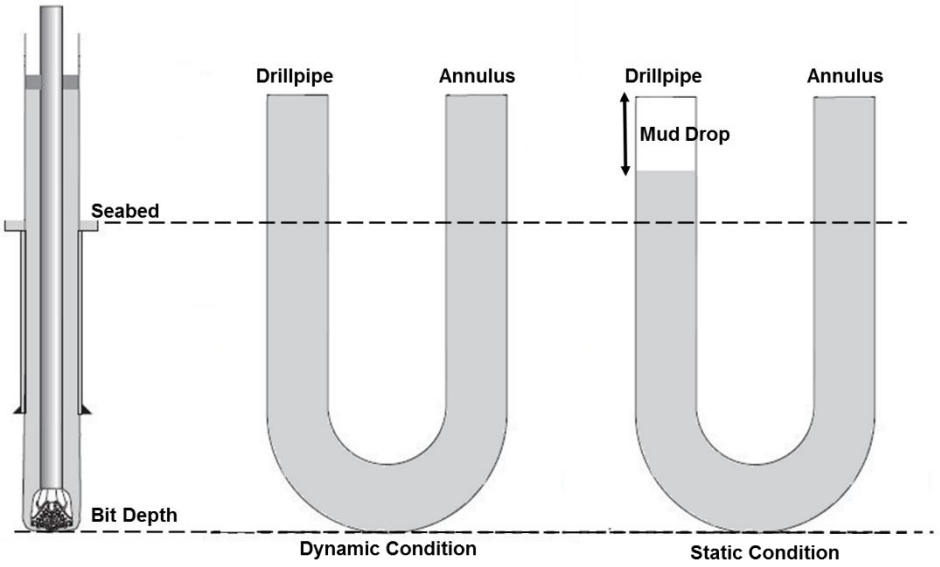

Figure 1.5 – The U-Tube Effect.

The density divergence creates a pressure imbalance between the drillsting and annulus when the pumps are not flowing. Therefore, the heavier mud free-falls and displaces the fluids inside the annulus until the system reaches the pressure balance. This

phenomenon is called the U-Tube Effect, as illustrated in Figure 1.5, understanding this is critical to the well control of the Dual Gradient Drilling, once the u-tube flow rate can mask influxes or circulation lost.

The purpose of this work is to understand the different parameters related to fluid dynamics in Dual Gradient Drilling. A hydraulic model contemplating the conservation of mass, momentum and energy and the density and viscosity model from Dr. Lima (1999) are used to simulate the dynamic behavior of the fluid. The Finite Element Method is used to discretize the system of partial differential equations, and the code is then implemented in Matlab®.

2 LITERATURE REVIEW

There are several works in the literature about hydraulic models for MPD procedures. This section is focused in an overview of the Dual Gradient Drilling and the Hydraulic model presented in the literature.

2.1 Dual Gradient Drilling Techniques

The UBO & MPD Glossary IADC, 2011 defines Dual Gradient Drilling, DGD, as “two or more pressure gradients within selected well sections to manage the well pressure profile”.

The concept was first introduced in the 1960s, although it was not implemented due to economic factors and the lack of technical need, since most of the wells were located at shallow waters and the conventional drilling fit this scenario. During the 70’s and 80’s a series of patents (Howell et al., 1977, Arnold, 1979, Beynet, 1981, Leach, 1989) were published, however, only in the middle 1990s, as the offshore exploration moved forward to deep waters, the need for better drilling techniques brought back the idea.

The DGD condition can be achieved by different techniques classified in Pumped-based, as the Subsea Mud Lift, or Dilution-based, as the Gas/Liquid Dilution or the Hollow Glass Spheres Injection, as illustrated at Figure 2.1. Both techniques are described in the next section.

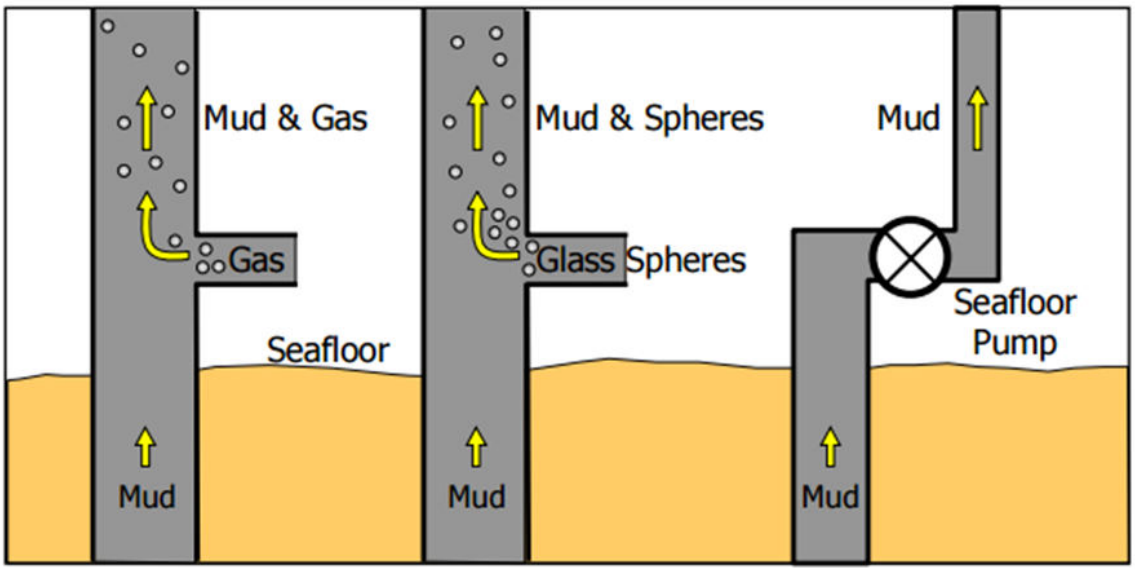

Figure 2.1 – Illustration of the DGD Techniques – A) Gas Dilution, B) Hollow Glass Spheres and C) Subsea Mudlift. (Cohen And Deskins, 2006)

Arrouj (2014) and Stødle (2013) present a detailed review about the current status of the DGD technology for deepwater and the future of the technique.

2.1.1 Subsea Mudlift Drilling

Rehm et al. (2008) defines Subsea Mudlift Drilling (SMD) as a MPD technique where the mud returns from the seafloor through small diameter lines, and the fluid inside of the marine riser has different density when compared to the drilling mud. A variation of the technique is the Riserless Mud Return (RMR), in which there is no marine riser connecting the drilling rig to the wellhead, so the mud is pumped to the surface or dumped at the seafloor.

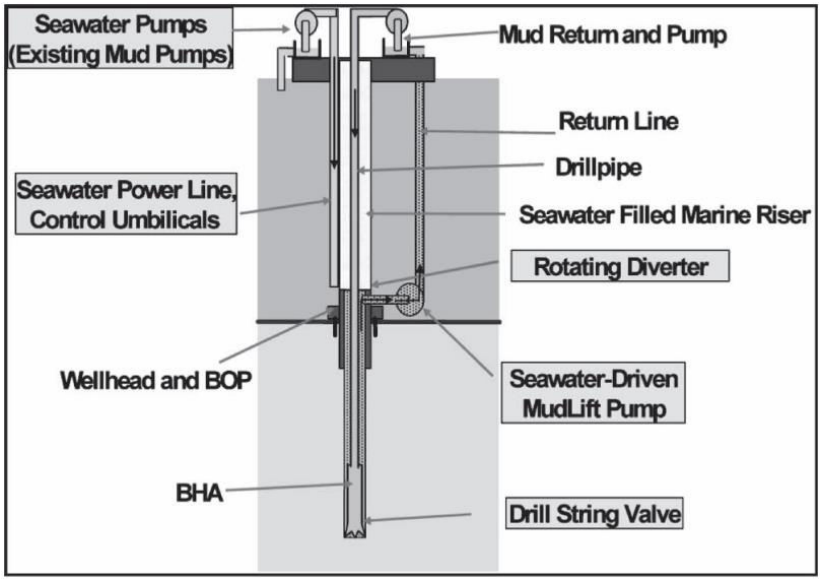

Figure 2.2 – Illustration of SMD System. (Schubert, Juvkam-Wold and Choe, 2006)

Schumacher et al. (2001), Smith et al. (2001) and Eggemeyer et al. (2001) present the pioneer project called Subsea Mudlift Joint Industry Project (JIP), in which different sectors of the deepwater industry united to, feasibly and safely, implement the DGD concept through the use of a positive displacement subsea mud pump to create the dual gradient. For more details about this project refer to Elieff (2006).

Although the Subsea Mudlift JIP was successfully tested in September 2001, Dowell (2010) describes it as an economic failure due to economic turbulence at the time and a lack of operators able to support the requirements needed to a DGD project. However, in 2006 members of the JIP decided to reevaluate the technical/economic scenario, which led to project that created Pacific Santa Ana, the first commercial DGD vessel the Gulf of Mexico.

Elieff (2006) uses a hydraulic simulator, developed by Choe (1995), to confirm the potential of RMR, in Top Hole Section, to mitigate shallow hazards, such as methane hydrates, shallow gas zones and shallow water flow.

Choe and Juvkam-Wold (1997a) and (1997b) present a comparison between the conventional drilling and RMR. They point the high costs of a long and large diameter riser as a disadvantage and limitation of the conventional drilling in deep water scenarios, while RMR has the reduction of casing point and less mud weight requirements as its advantages. Although, when the paper was published, the technique had unsolved problems, such as equipment and technologies.

Mir Rajabi et al. (2012) describe the EC-Drill system developed by AGR, Figure 2.3. It is the first modified riser joint with an outlet that feeds a multiphase subsea pump, diverting the flux from the annular to the surface throughout small diameter mud return hose. Also, it includes an accurate multiphase flowmeter, allowing the quick detection and control of influxes and losses, and a pressure sensor for the estimation of the mud level inside of the riser.

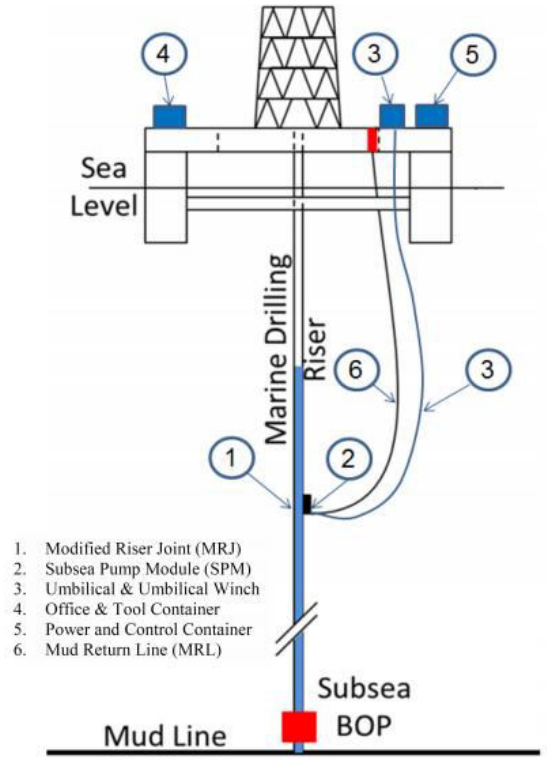

Figure 2.3 – EC-Drill's Scheme. (after Stave, 2014)

Ziegler, Ashley, et al. (2013) report EC-Drill first test, in May 2012, on an ultra-deepwater well (7400 ft. water depth). The test concluded that the system is capable to manage the level inside the riser annulus, consequently, being capable to managed BHP. It also successfully allowed cementing operations and well control.

In another work, Ziegler, Sabri, et al. (2013), described the evolution of the EC-Drill system, observe in Figure 2.4 that the control system evolved from the RMR pump control system until fully Controlled Annular System.

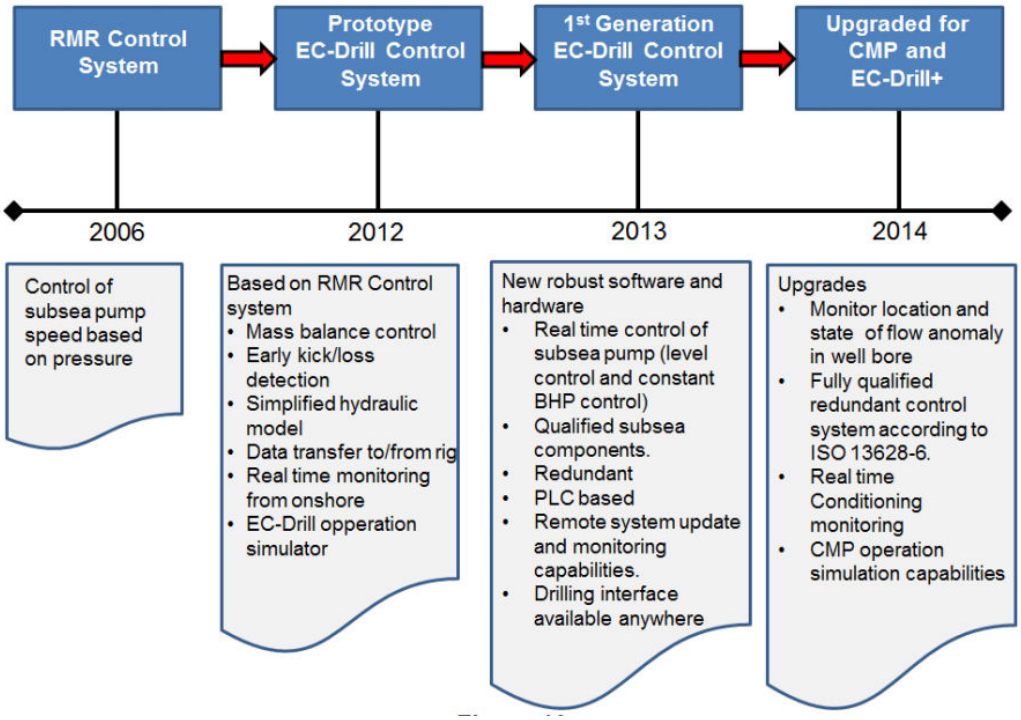

Figure 2.4 – Development Stages of the Controlled Annular System. (Ziegler, Sabri, et al., 2013)

The Low Riser Return System (LRRS) devolved by Ocean Riser system is similar to the EC-Drill system, however the marine riser is partly-evacuated. In other words, it is filled with gas at almost atmospheric pressure. The system and well control procedures are discussed by Falk et al. (2011) and Fossli and Sangesland (2010).

2.1.2 Hollow Glass Spheres

In this technique, Hollow Glass Spheres, Figure 2.5, are mixed in slurry and pumped down into the riser annulus, as a lightweight additive, to reduce the mud density.

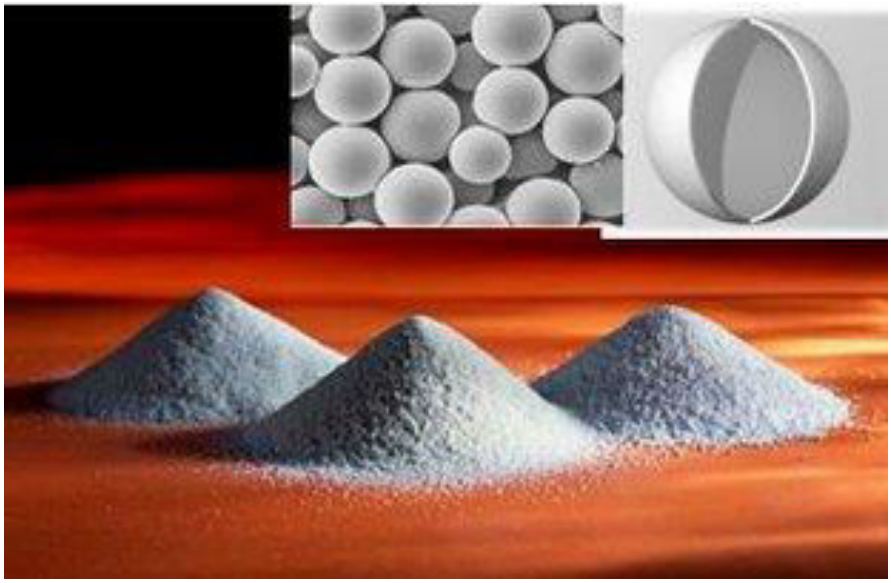

Figure 2.5 – 3M™ Glass Spheres, Density of 0.38 g/cc and an Isostatic Crush Strength of 4,000 psi.

The concept has been used for cementing for decades, and it was first applied and tested for drilling fluid by Maurer Technology Inc. (Medley, Maurer and Garkasi, 1995). And most recently, the department of Energy also created a project to investigate the application of this idea for drilling proposes (William, 2011).

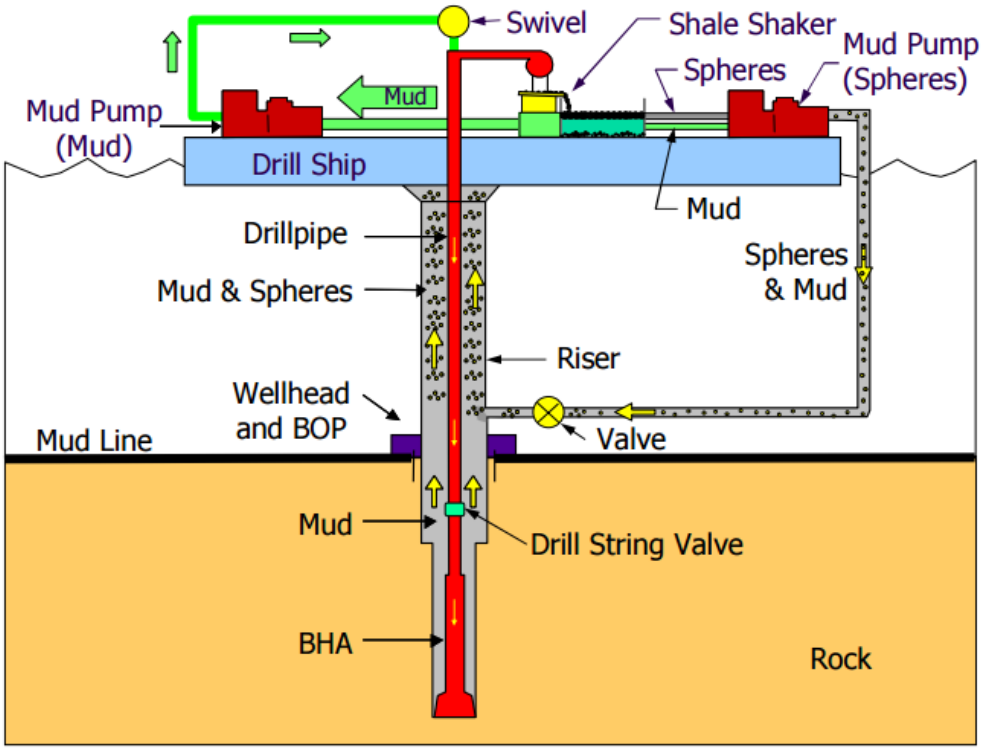

Figure 2.6 – Hollow Glass Spheres Scheme. (Cohen and Deskins, 2006)

Figure 2.6 illustrates the system to mix, inject and separate the hollow spheres from the drilling mud. The mixed slurry is injected in the base of the riser annulus and is carried with the drilling fluid to the shaker, where it is separate from the mud.

Vera Vera (2002) evaluates the potential use of hollow spheres in the DGD. The author developed a spreadsheet to model the hydraulic effects of the injection of hollow spheres at the sea floor depth, being able to identify features as particles size, collapse pressure and concentration for a desired mud density. It is worth noting that when using drilling mud to carry the spheres, system does not require any additional equipment at the seafloor.

According to Cohen and Deskins (2006) small diameter spheres are difficult to remove from the mud, then large spheres (> 100 microns) are required, which also contribute to lower the mud viscosity. Another important aspect of the hollow sphere is incompressibility, which produce a linear pressure gradient.

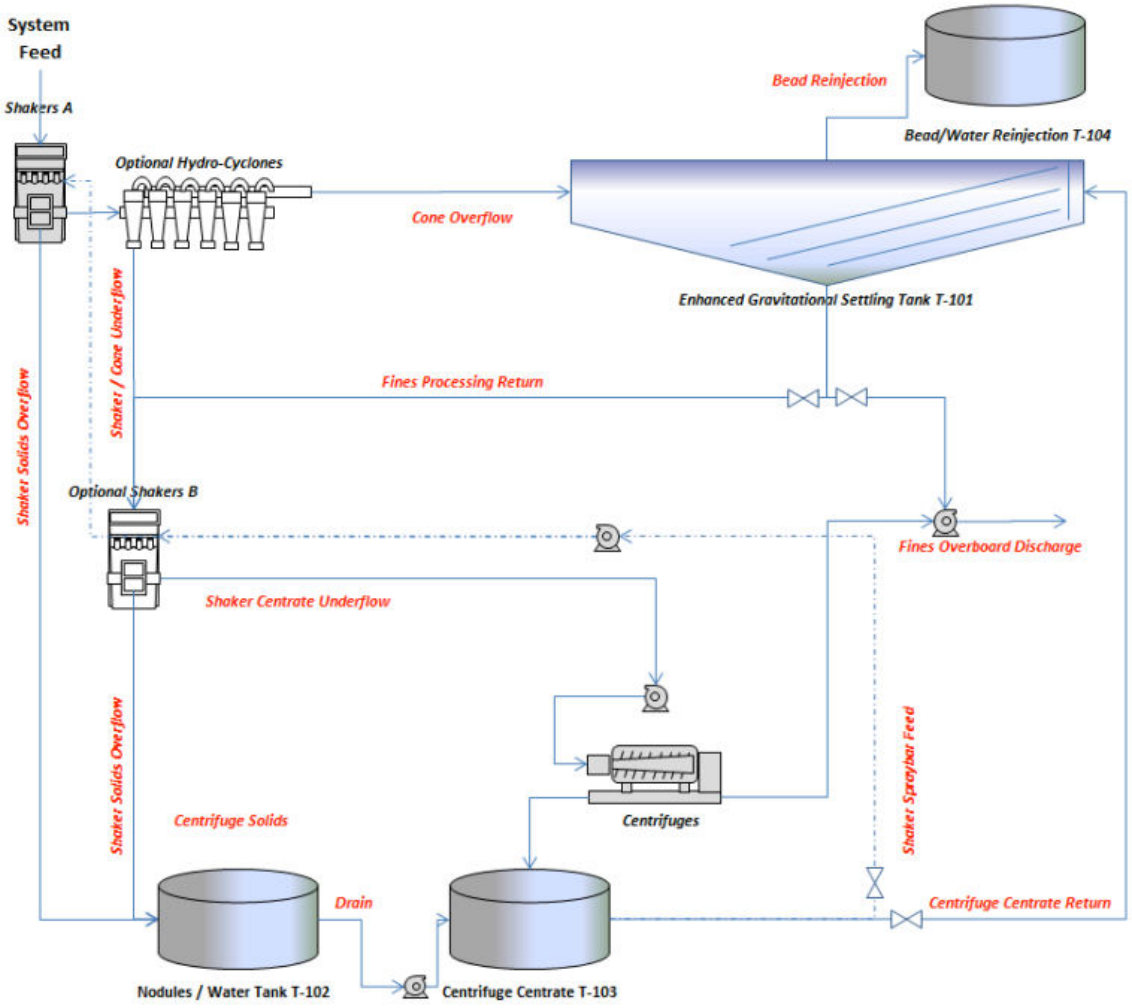

Figure 2.7 – Illustration of Separation and Recovery System. (Halkyard, Anderson and Maurer, 2014)

Halkyard, Anderson and Maurer (2014) talk about the most recently separation and recovery techniques for hollow glass spheres, as illustrated in Figure 2.7. The mud passes through a series of hydro-cyclones, shakers and gravitational tanks to an efficient solid-liquid separation. With the current technology, the process depends upon the density, strength and particle size distribution.

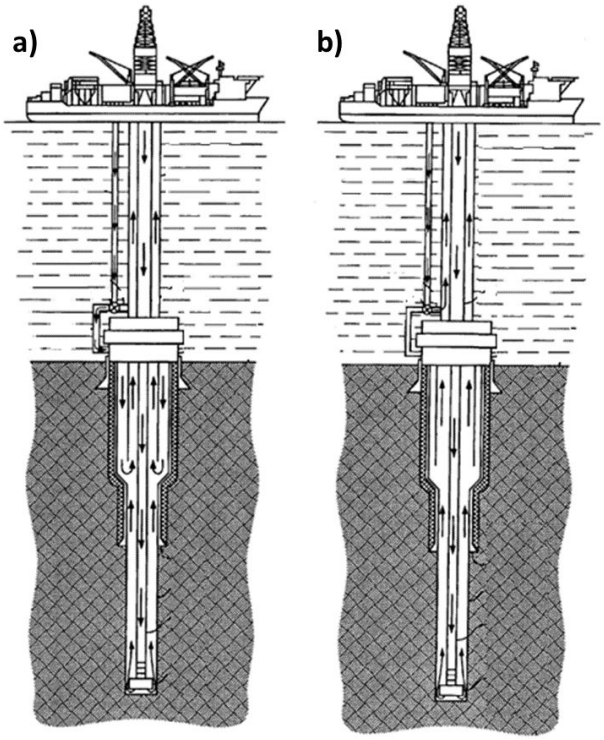

Figure 2.8 – Fluid Dilution Technique. a) Injection Below BOP, b) Injection Above BOP. (after deBoer, 2005)

2.1.3 Riser Dilution

The Riser Dilution uses the same principle of the Hollow Spheres Injection, but it uses gas or liquid instead. deBoer (2005) registered the first patent describing the process. This approach is illustrated in Figure 2.8, observe that a light fluid is pumped

down through the charging line until the mixing point, where the light fluid is mixed with the drilling fluid inside the annulus. The injection point can be either, below or above the Blow out Preventer (BOP) stack.

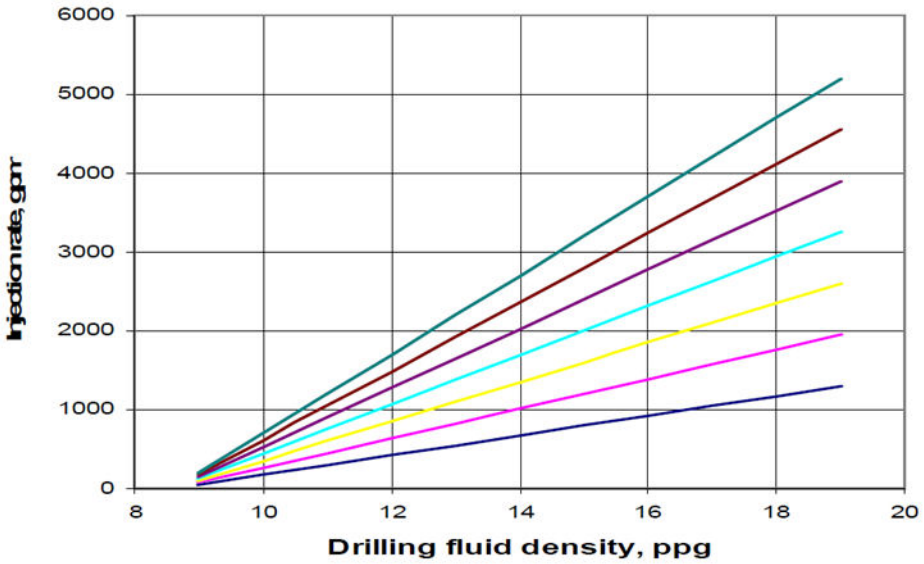

Figure 2.9 – Required Injection Rate to Dilute the Fluid to a Certain Density. (Okafor, 2007)

It is important to keep the mud density, above the seabed, equal to the sea water density, therefore, a right combination of mud weight and injection rate can attend this criteria. Okafor (2007) elaborated a spreadsheet to investigate this problem. The results are presented in form of charts correlating the injection rate, mud weight and flow rate, as observed in Figure 2.9 and Figure 2.10.

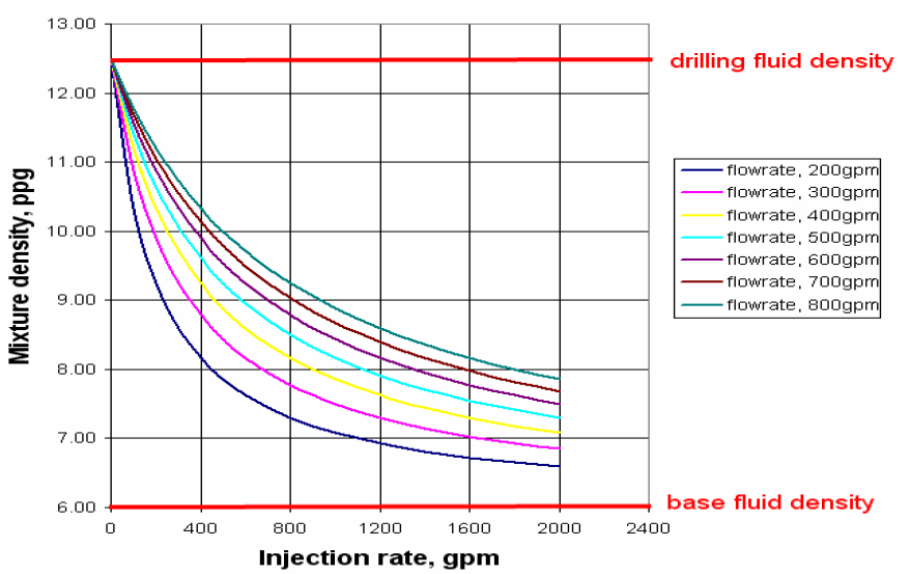

Figure 2.10 – Effects of the Injection Rate in the Fluid Density in the Riser. Base Fluid 6.0 ppg, Drilling Fluid 12.5 ppg. (Okafor, 2007)

2.2 Hydraulic Models

Lima (1999) developed a one-dimensional numerical model based on the conservation equations to simulate the flow of Synthetic-Based-Mud (SBM) in a RMR system. The density and viscosity model were correlated from an experimental work in alliance with Petrobras. A sensitive analysis showed an increment of 0.5 ppg in the fluid

density at the bottom and a quick temperature drop. Both facts are critical for the estimation of the drilling hydraulics.

Zhang (2000) research was similar to Lima (1999) although the Riser Dilution technique was used instead. The viscosity model incorporates not only the effects of pressure and temperature, but also the density and viscometer readings.

Gaup (2012) used a hydraulic model based on a set of 6 dimensionless equation described by Crespo, Ahmed and Saasen (2010) . The simulation reproduced the Macondo accident scenario using DGD technique, showing that incidents that led to the disaster could have been easily discovered in earlier stages if DGD was being used.

Haj (2012) use the Advection Upstream Splitting Method (AUSMV) to simulate a Drift Model that capture the dynamics effects of the LRRS. It considers a two phase flow and use the conservation equation to predict the dynamics during a Kick event. The results proved the ability to control the kick without pump a kill mud, using only the subsea pump as a choke. Sigurjonsson (2012) studied how hydraulics and mud level effects the annular pressure in the Low LRRS.

Kaasa et al. (2011) elaborate a simplified hydraulic model in order to apply the control theory. The model is based on the balance equations, density model and viscosity model. A series of assumption were applied to reduce the complexity of the system, so it could conform to the control system bandwidth. The assumptions are:

1. The flow can be treated as one-dimensional along the flow path, i.e, time-averaging the fluctuations due turbulence.
2. Flow is radially homogenous, i.e, average properties over cross sectional area.
3. Fluid is incompressible, i.e, neglecting the time-variance of the density in the momentum equation.
4. Assume viscosity is time independent.

Time (2014) use the Kaasa et al. (2011) model to study the effect of the DGD system in the control of the BHP during connection operations. The results were compared to the existent MPD control system, proving that the DGD could control the pressure in much faster than the MPD.

2.3 U-Tubing Effect and Drillstring Safety Valve

The density imbalance between the drillstring and the annular creates a pressure differential which causes the drilling mud to flow even when the pumps are off, in other words the mud free fall inside of the drillpipe. This phenomenon is known as U-Tube Effect, and it can represent serious risk to the well control during the connection operation, since it can interfere in the BHP and disguise kicks or fluid lost.

Extensive studies have been performed on the topic. Schubert (1999) demonstrates that several factor contribute to the free fall rate. Which include water depth, mud density, mud viscosity, drillstring diameter, bit nozzles, and other pressure restrictions.

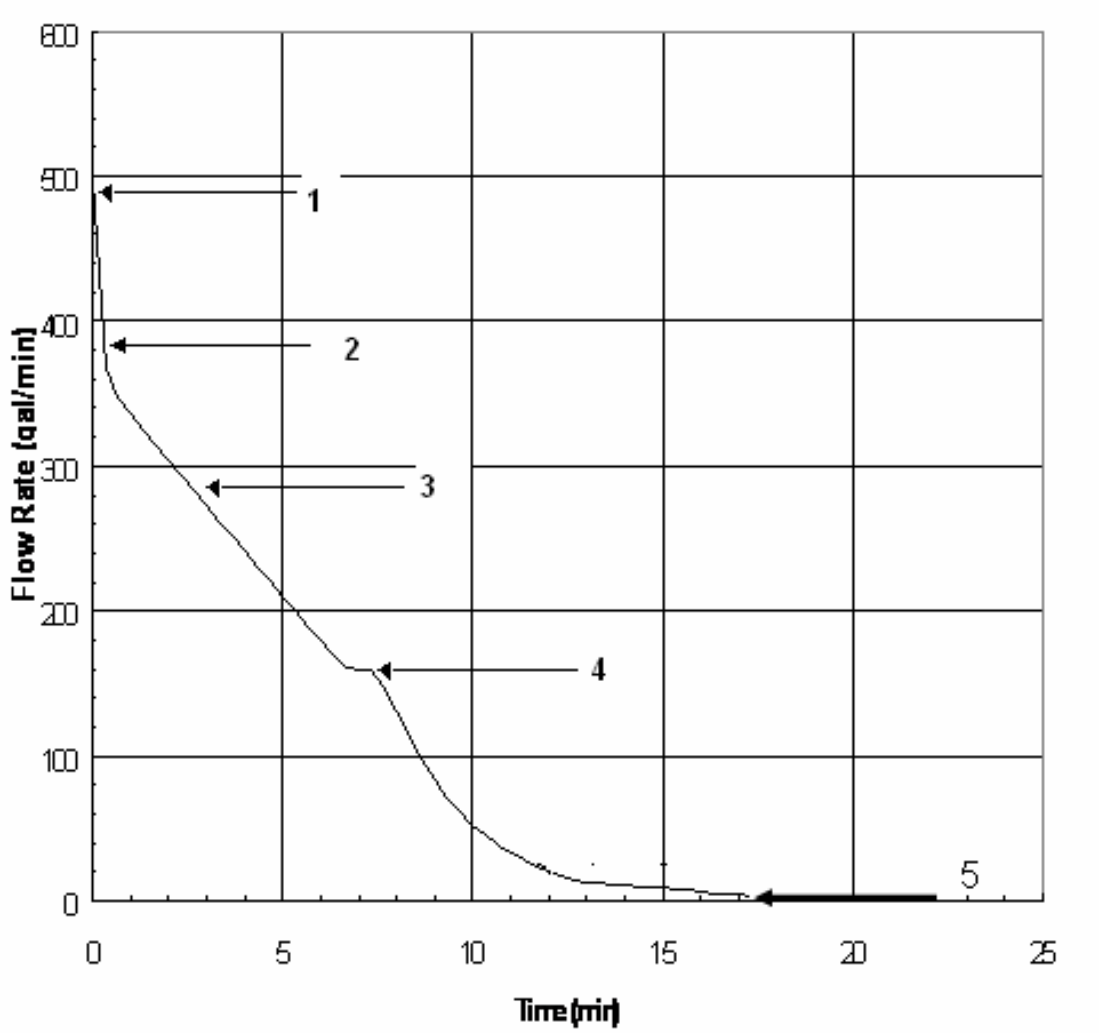

Figure 2.11 – U-Tube Effect Pattern. (Choe, Schubert and Juvkam-Wold, 2007)

According to Johansen (2000) there are few stage during the U-tube Effec for SMD system, Figure 2.11. The process is described the Choe, Schubert and Juvkam-Wold (2007), it initial with the original circulation rate when the pumps are shut down (1), the dynamics effects of the imbalance start to act an fluid level starts to drop (2), which decreases the driving force of the phenomenon (3), the flow rate reduces and the flow regime changes from turbulent to laminar (4), and finally the system reaches the equilibrium (5).

Figure 2.12 and Figure 2.13 show the effects of drillpipe inner diameter and water depth over the free fall rate. Note that can take up to 20 min to system stabilize and the rate of as close as the initial circulation rate can take place for few minutes.

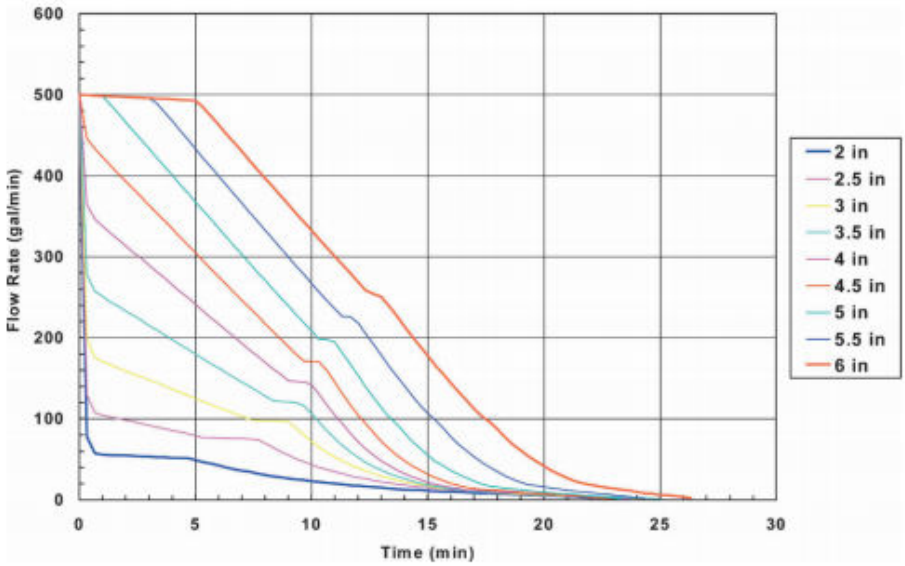

Figure 2.12 – U-Tube Rate for Different Drillpipe Diameters. (Johansen, 2000)

Seland (1999), Vera Vera (2002) and Okafor (2007) studied the effects the U-tube in the RMR, Hollow Glass Spheres Injection and Liquid Injection respectively. In all the cases the free fall behavior was similar to observed in the SMD.

The U-Tube effect can be avoid with a special value, placed in the bottomhole assembly, known as the Drillstring Safety Valve (DSV), Figure 2.14. It consist of a spring value that that supports the hydrostatic pressure of the column of mud above it.

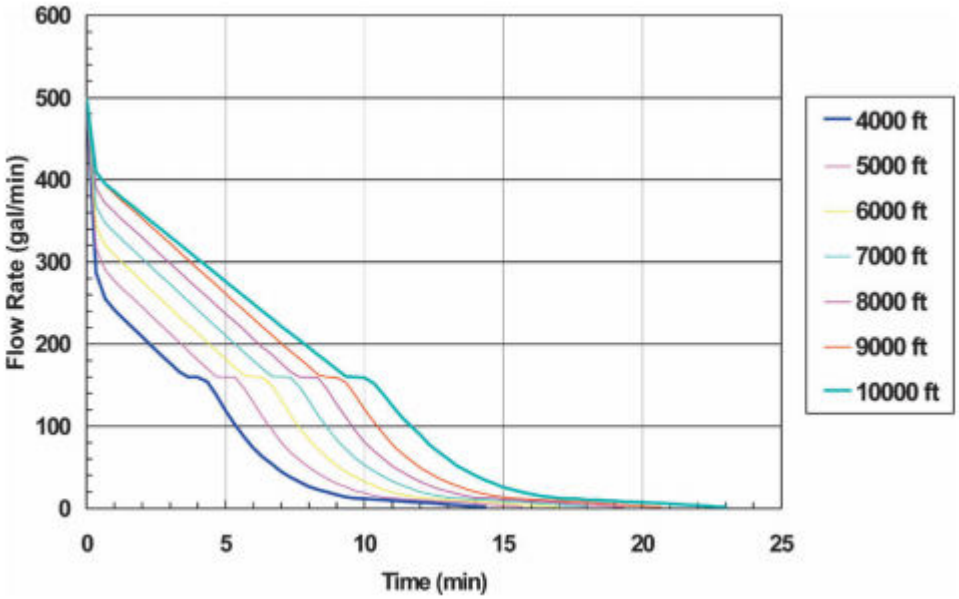

Figure 2.13 – U-Tube Rate for Different Water Depths. (Johansen, 2000)

Oskarsen, 2001 modeled the opening process and the pressure drop across the valve. The compressibility of the spring can be adjusted at the surface and it will control

the opening process once the valve is put in place. The DSV was developed by Gonzalez and Smits (2002) and its design, test and implementation is described by Goldsmith (1998).

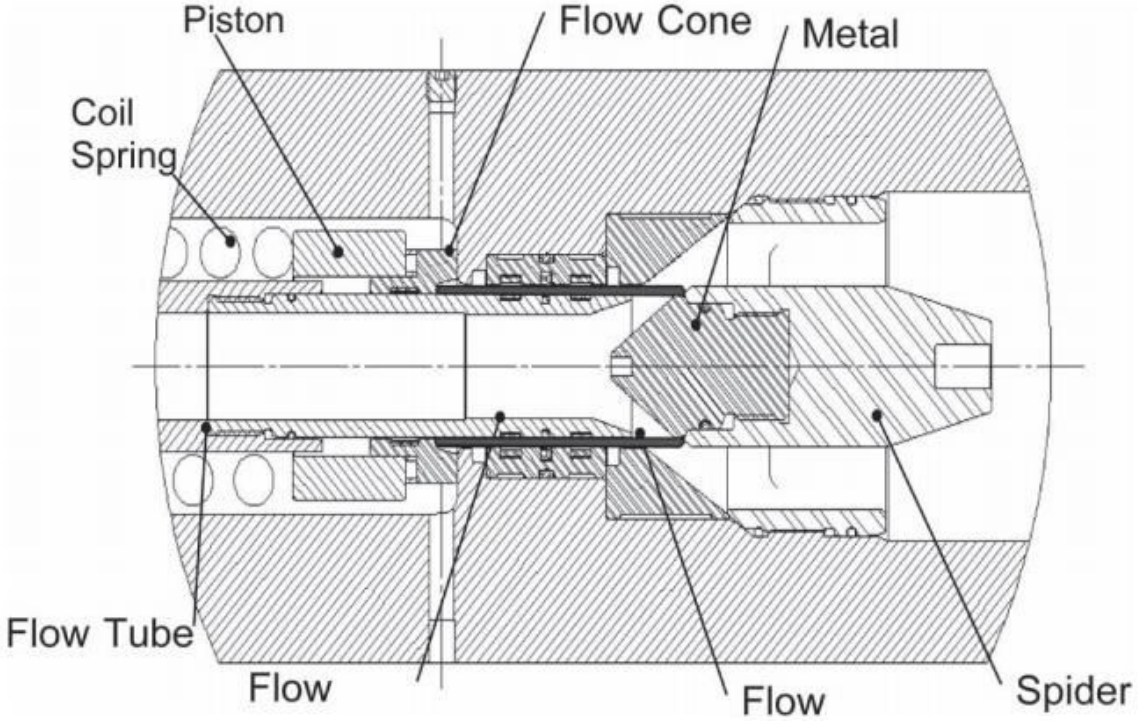

Figure 2.14 – Drillstring Safety Valve. (Oskarsen, 2001)

3 HYDRAULIC MODEL

This section will discuss the equations governing the fluid dynamics in the Dual Gradient Drilling. The hydraulic model is based on the work of Dr. Heitor Lima (1999).

An advanced model should be able to reproduce a large number of complexity in the drilling system, however it makes the simulation computationally expensive and challenging to implement, which stimulate the use of simplified hydraulic models (Kaasa et al., 2011).

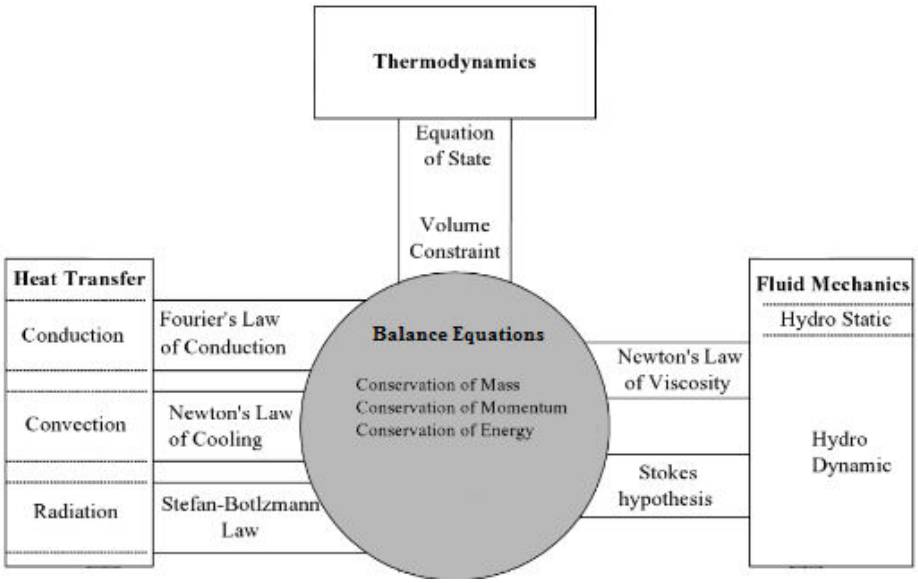

Figure 3.1 – Scheme of a Hydraulic Model. (after Massoud, 2005)

A simplified model must have in its bases the set of fundamental balance equations (mass, energy and momentum), and closure equation, such as Constitutive Equations and Equation of State (EOS), as well as Initial and Boundary Conditions to be considered well purposed. Figure 3.1 illustrates a scheme a hydraulic model.

3.1 Balance Equation

The balance equations come from the observation that mass and energy must be conserved in a control volume. Therefore, consider a volume, Ω, bounded by the surface, $\partial\Omega$, and arbitrary specific property, ϕ.

The rate of change is given by the total flux through the boundary and the internal source/sink. The equation that represents this balance is

$$\frac{\partial}{\partial t}\left(\int_{\Omega}\rho\phi dx\right) = -\iint_{\partial\Omega}\rho\phi\left(\mathbf{u}.\mathbf{n}\right)ds + \iint_{\partial\Omega}\boldsymbol{\Gamma}.\mathbf{n}ds + \int_{\Omega}Qdx \qquad 3.1$$

where the left-hand side is the rate of change of the property. The first term in right-hand side is the advective flux, the second term is the diffusive flux and the last term is the rate of generation (source/sink). Here $\mathbf{u}$ is the velocity field, $\boldsymbol{\Gamma}$ is the flux vector and Q is the generation rate per unit of volume.

Applying the Divergence Theorem in the first two term of the left-hand side, it is possible to rewrite the equation 3.1 as:

$$\int_{\Omega}\left[\frac{\partial}{\partial t}(\rho\phi)+\nabla.(\rho\phi\mathbf{u}-\mathbf{\Gamma})-Q\right]dx=0 \qquad 3.2$$

where $\nabla.$ is the divergence operator.

As equation 3.2 must apply for any Ω, hence the integrant must be zero, which leads to the differential form of the conservation equation:

$$\frac{\partial}{\partial t}(\rho\phi)+\nabla.(\rho\phi\mathbf{u})=\nabla.\mathbf{\Gamma}+Q \qquad 3.3$$

The equation above is the generalized balance equation and applies for any property ϕ.

Table 1 – Examples of Quantities that Satisfy the Balance Equation

	Property (ϕ)	Flux (Γ)	Source (Q)
Continuity	1	0	0
Momentum	$\mathbf{u}$	Momentum Flux	$\rho\mathbf{g}$
Energy	$e+\mathbf{u}^2/2$	Heat Flux	$\dot{q}$

Table 1 provides the expression for the property, flux and the source/sink term for the equation of Continuity, Momentum and Energy. The flux is given by Constitutive Equation and will be discussed in the next sections. The specific enthalpy, e, and specific mass, ρ, are given by Equations of State and are discussed in the section 3.3.

Applying the values of the first line of Table 1 into 3.3 leads to the Continuity equation as

$$\frac{\partial \rho}{\partial t} + \nabla.\left(\rho \mathbf{u}\right) = 0 \qquad 3.4$$

3.2 Constitutive Equations

Constitutive Equations are the Laws of Physics that describe how materials respond to a stimulus. The most known constitutive equations are the Fick's Law of Diffusion, Fourier's Law of Thermal Conduction, Newton's Cooling Law, Ohm's Law of Electric Conduction and the Stress and Strain relationships, such as Hook's Law of Elasticity for solids or Newton's Law of Viscosity for fluids.

In the essence, most of constitutive equations are derivative of an empirical observation, and relate a material property, such as viscosity, thermal conductivity and heat exchange coefficient, to physical quantities.

3.2.1 Momentum Flux Tensor – Stress-Strain Relationship

For the purpose of this study, the Stress-Strain relationship for fluids will be presented in details because of its importance in describing the fluid dynamics of drilling fluids.

For starts, let's define the Cauchy's Stress Tensor as:

$$\mathbf{T} = -p\mathbf{I} + \boldsymbol{\tau} \tag{3.5}$$

in which $\mathbf{T}$ is the Stress Tensor, p is hydrostatic pressure, $\boldsymbol{\tau}$ is the Shear Stress Tensor and $\mathbf{I}$ is the identity matrix.

The Newtonian Fluid is the most simplistic relationship between Shear Stress and Strain Rate (Deformation Rate), $\dot{\gamma}$. Equation 3.6 represents this relationship, observe that the properties are linearly proportional.

$$\boldsymbol{\tau} = \eta\dot{\boldsymbol{\gamma}} \tag{3.6}$$

The proportionality constant is called viscosity, η, it is a function of pressure and temperature, and it is related to the resistance of the material to the deformation when shear stress is applied to it. The definition of Strain Rate is

$$\dot{\boldsymbol{\gamma}} = \frac{1}{2}\left(\nabla\mathbf{u} + \nabla\mathbf{u}^{T}\right) \tag{3.7}$$

in which first term, $\nabla \mathbf{u}$, is the velocity gradient tensor and the second term is its transpose.

Although many fluids are classified as Newtonian fluids, the drilling mud is a complex mixture of particles in suspension and emulsion, so a simplistic model does not provide the properties required to safely and efficiently drill a well. Therefore, drilling fluids are classified as Non-Newtonian fluid, which means that Shear Stress is not linearly proportional to the Strain Rate.

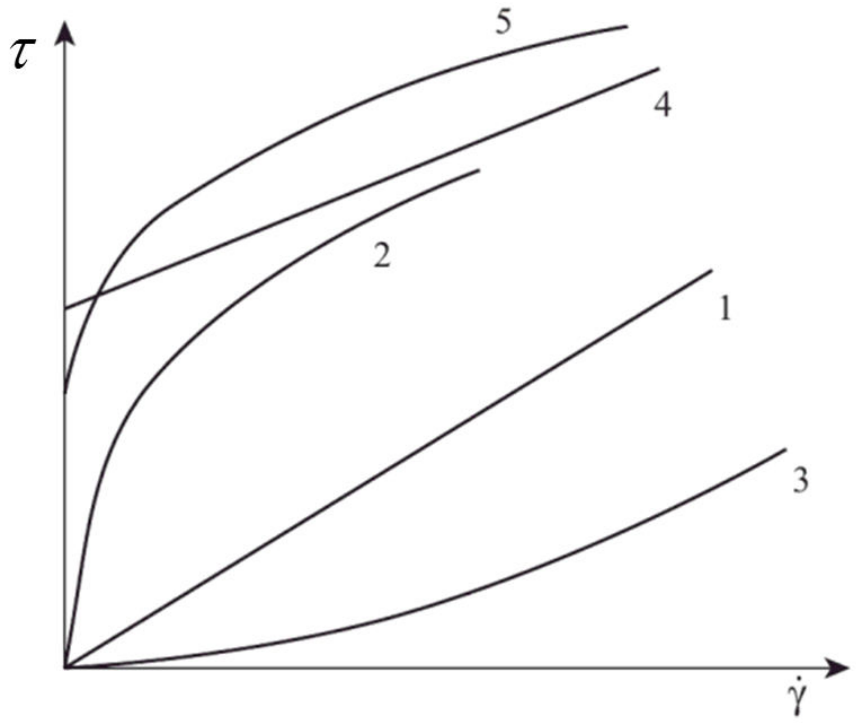

Figure 3.2 – General Illustrate of Shear Stress and Shear Rate Relationship. (1) Newtonian Fluid, (2) Shear Thinning, (3) Shear Thickening (4) (5) Fluids With Yield Stress. (after Mewis and Wagner, 2012)

According to Hartnett and Cho (1998) the Non-Newtonian fluids are classified into purely viscous, time dependent and viscoelastic, with the Newtonian Fluid as subclass of the purely viscous.

The purely viscous fluids are subdivided as in Newtonian, shear thinning or pseudoplastic, shear thickening or dilatant and viscoplastic. Observe the non-linearity in curves (2) and (3) in Figure 3.2, in the first, the apparent viscosity (ratio between shear stress and strain rate) decreases with increasing strain rate. In second, it is the opposite case and the apparent viscosity increases with decreasing the strain rate. Those curves are known as the Power Law, because of the shape of the function that represents them:

$$\boldsymbol{\tau} = K\dot{\boldsymbol{\gamma}}^{n} \tag{3.8}$$

in which n is the flow behavior index ($n<1$ shear thinning, $n>1$ shear thickening) and K is the flow consistency index.

Yet in the subclass of purely viscous fluid, the viscoplastic fluids are those in which there is a minimum amount of stress required to initiate the flow, as in curves (4) and (5). This point is called Yield Stress, $\boldsymbol{\tau}_{\mathrm{y}}$. Bingham (4) and Herschel-Buckley (5) are the most common models for these fluids, being represented by equation 3.9, wherein $n=1$ is the Bingham Model.

$$\boldsymbol{\tau} = \boldsymbol{\tau}_{\mathrm{y}} + K\dot{\boldsymbol{\gamma}}^{n} \tag{3.9}$$

In the time dependent fluid, the shear stress is not only function of the strain rate, but also of the duration of its application. Those fluids can be subdivided into Thixotropic and Rheopectic. Mewis and Wagner (2012) define Thixotropy as the "continuous decrease of viscosity with time when flow is applied to a sample that has been previously at rest, and the subsequent recovery of viscosity when the flow is discontinued." Tomsic (2000) defines rheopectic substance as "a fluid whose apparent viscosity increases with time at any constant shear rate." The Figure 3.3 illustrates the time dependent behavior, observer the hysteresis aspect of the curves.

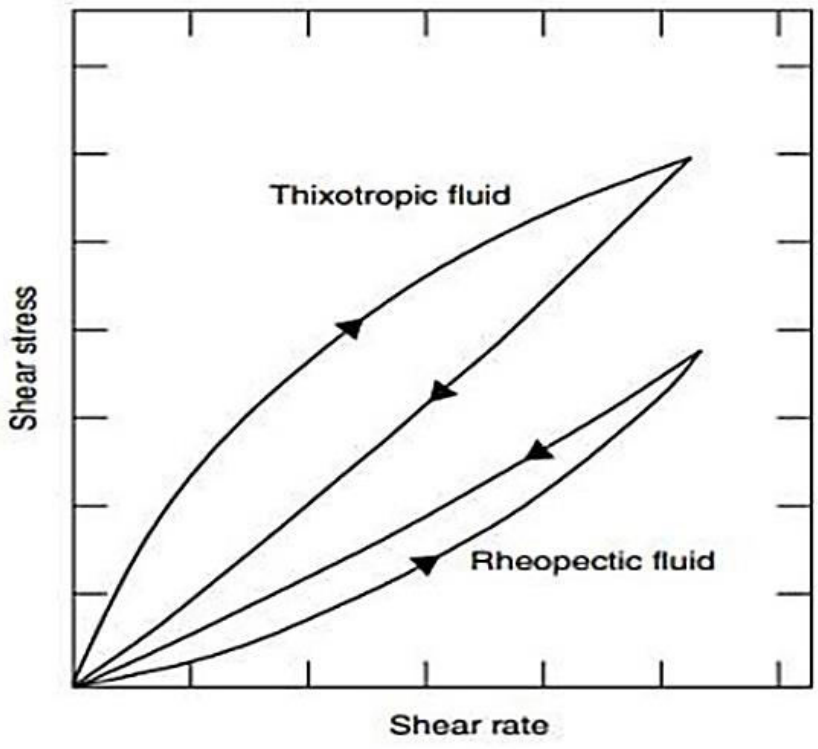

Figure 3.3 – Time Dependent Fluid Behavior.

Viscoelastic fluids are those which have elastic and viscous characterizes. In other words, the fluid presents properties similar to the Hook Law of Elasticity, as well as to the Newton Law Viscosity. This means that part of the deformation is recovered upon removal of the stress, and the stress is gradually dissipated.

The viscosity model is very important to correctly address the characteristics of the fluid. The viscosity is related to the thermodynamic state of the fluid. For example, the viscosity of gas and vapor tends to increase with the increasing o temperature. Whereas the opposite occurs with liquid, its viscosity decreases with the increasing of temperature.

Lima (1999) creates a viscosity model for synthetic mud based on rotational viscometry for high pressure and high temperature. The data from the viscometer were used to obtain flow behavior and consistency index and those were correlated with pressure and temperature. The model includes both situations where the fluid is flowing inside the drillpipe or the annulus.

$$\begin{aligned} n_{dp} &= \begin{cases} 0.78 & T < 120\,^{\circ}F \\ 0.63 + 0.00122T & 120 < T < 300\,^{\circ}F \end{cases} \\ K_{dp} &= \left(0.15 - 0.0007\,p\right)\ln\left(T\right) + 0.0036\,p - 0.00863 \quad T < 150\,^{\circ}F \end{aligned} \tag{3.10}$$

Equation 3.10 show the correlation for the inner flow, and equation 3.11 show the correlation for the annular flow.

$$n_{an} = \left(0.302 + 0.000874T - 8\times10^{-6}T^2\right)\exp\left(2.7\times10^{-5}\,p\right) \quad T < 150^{o}F$$
$$K_{an} = 23.573 + \frac{616.22}{T} \quad T < 150^{o}F \qquad 3.11$$

Given the above, it is possible to represent the Momentum Balance Equation combining equations 3.3, 3.5 and Table 1:

$$\frac{\partial \rho \mathbf{u}}{\partial t} + \nabla.\left(\rho \mathbf{u}\mathbf{u}\right) = -\nabla p + \nabla.\boldsymbol{\tau} + \rho \mathbf{g} \qquad 3.12$$

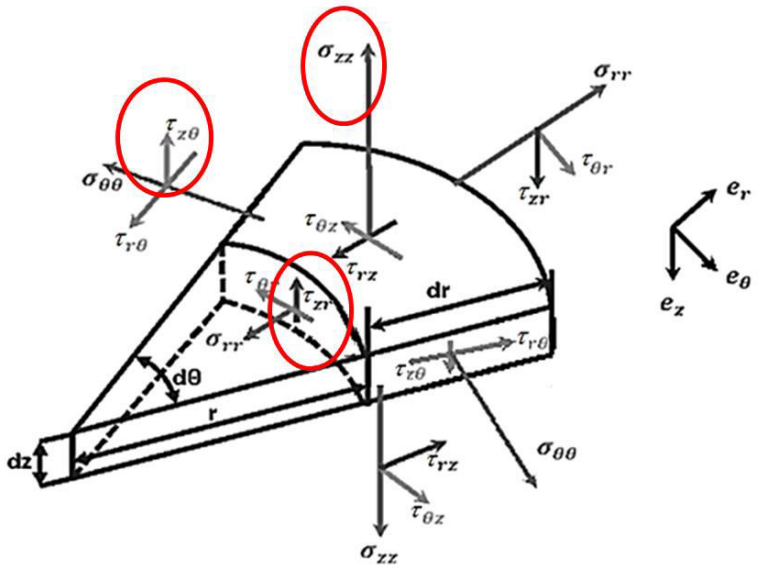

Figure 3.4 – Cylindrical Components of the Shear Stress Tensor.

Now, consider the hypothesis of one-dimensional flow, which means that there is only one velocity component, the axial velocity, and that all properties change only with the axial direction. Observe in Figure 3.4, the axial components of the Shear Stress Tensor are $\tau_{zr}, \tau_{z\theta}, \sigma_{zz}$, where the axial and circumferential components can be neglected, in other words, there is only flux of momentum due to shear stress in the radial direction.

Calculating the divergent of the shear tensor in the equation 3.12 as:

$$\nabla.\boldsymbol{\tau} = \frac{\int_{\Omega} \nabla.\boldsymbol{\tau} dx}{\int_{\Omega} dx} \qquad 3.13$$

Applying the Divergence Theorem in the numerator and solving the integral in the denominator:

$$\nabla.\boldsymbol{\tau} = \frac{\oiint_{\partial\Omega} \boldsymbol{\tau}.\mathbf{n} ds}{AL} \qquad 3.14$$

where A is the cross-sectional area and L is the length of the control volume. As there is only flux of momentum in the radial direction, the surface integral in equation 3.13 become

$$\oiint_{\partial\Omega} \boldsymbol{\tau}.\mathbf{n} ds = \tau_{rz} \int r d\theta dz = 2\pi r L \tau_{rz} \qquad 3.15$$

Substituting equation 3.15 into 3.13 leads to

$$\nabla.\boldsymbol{\tau} = \frac{\pi d}{A}\tau_{rz} \tag{3.16}$$

As mentioned before, the drilling fluids are a complex mixture of suspension of solids and emulsion and the adoption of a single model cannot completely describe the affects that different physical properties have over the Shear Stress. Therefore, most of the time, engineers appeal to empirical correlations and dimensional analyzes, that contemplates the different features of each model. One examples is the equation

$$\tau_{rz} = f\frac{\rho u^2}{2} \tag{3.17}$$

where f is the Fanning Friction factor, that is function of the Reynolds Number and Relative Roughness, and it is used for non-Newtonian fluids. For Newtonian fluids, the Moddy Friction factor, that is four times the Fanning Factor, should be used.

The API RP 13D (2009) provide a procedure to calculate the friction factor as function of fluid properties and viscometer reading, and will be used in this work.

Consider the steady-state hypothesis and the assumption made by Kaasa et al. (2011). So, combining equation 3.16 and leads to the final form of the Momentum Equation for this model:

$$\rho u\frac{\partial u}{\partial z} = -\frac{\partial p}{\partial z} + 2\frac{f\rho u^2}{d} + \rho g \tag{3.18}$$

Observe that the vector notation was removed because of the one-dimensional hypothesis.

3.2.2 Heat Flux – Heat Transfer Mechanisms

The constitutive equation governing heat flux depends on how the heat is transferred in the process, in other words the heat transfer mechanisms, that can be classified as Conduction, Convection and Radiation, each one with a characteristic law.

Fourier's Law of heat diffusion perhaps is the most common relation between rate of heat transfer and the temperature. It states that the heat flux is proportional to the temperature gradient:

$$q'' = -\kappa \nabla T \tag{3.19}$$

where the proportionality factor, κ, is the called Thermal conductivity, the minus sign appears because of the flux occurs in the opposite direction of the temperature gradient.

The Newton's Cooling Law describes the heat transfer by convection. In this mechanism the heat flows due to the bulk motion of a fluid. It can be classified in Natural Convection, when the fluid motion in caused only by the temperature gradient, and Forced Convection, when fluid motion is caused by different factor, such as pressure gradient. Similarly to the previous mechanism, the heat flux is proportional to the temperature gradient:

$$q'' = h\Delta T \qquad 3.20$$

where the proportionality factor, h, is the called Heat Transfer Coefficient.

The Radiation mechanism is not important to this study and will not be discussed here.

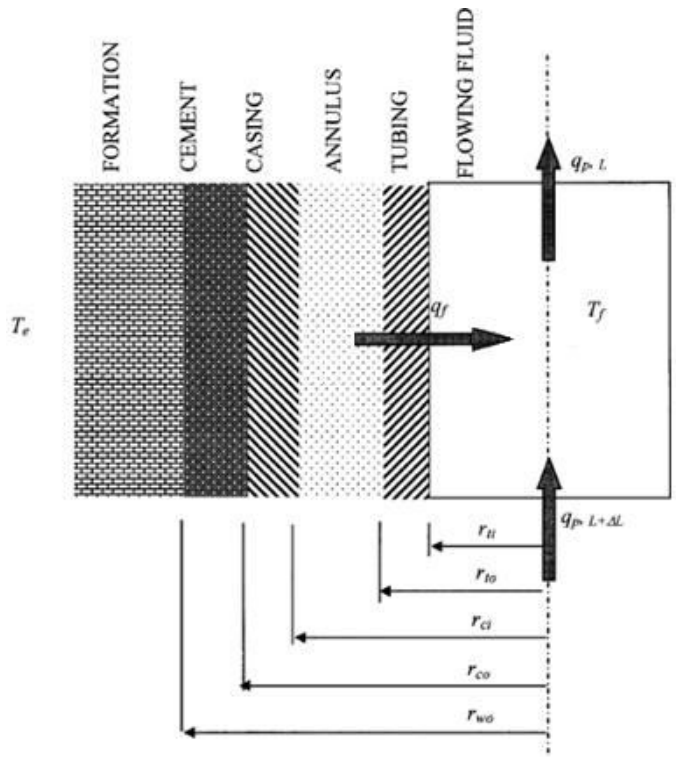

Figure 3.5 – Temperature Flux For a Control Volume. (after Oskarsen, 2001)

The effects of Conduction and Convection can be combined over the Overall Heat Transfer Coefficient. According to Oskarsen (2001), this is most difficult parameter to estimate, because, below mud line, it depends on the variety of factors, such as drillstring configuration, previous completion and wellbore geometry.

In order to estimate the Overall Heat Transfer Coefficient, let's start estimating the Heat Rate by the surface integral of the Newton's Cooling Law, note that the heat flux in the radial direction, Figure 3.5, therefore

$$\dot{q} = \iint_{\partial\Omega} q'' ds = 2\pi r L h \Delta T \tag{3.21}$$

Isolating the temperature difference

$$\Delta T = \frac{\dot{q}}{2\pi r h L} \tag{3.22}$$

Similarly for the Fourier's Law

$$\Delta T = \frac{\dot{q}}{2\pi L} \frac{\ln\left(OD/ID\right)}{\kappa} \tag{3.23}$$

where od and id are the outer and inner diameter, respectively.

Observe in Figure 3.5 that the heat flows from the formation to the drillstring. So the heat rate flowing from the formation is calculated based on the Infinite Line-Source solution,

$$\Delta T = \frac{\dot{q}}{2\pi rL}\frac{f(t)}{\kappa} \tag{3.24}$$

where $f(t)$ is a function of time analogous to the flux function for the van Everdingen-Hurst constant heat solution of the transient flow. Oskarsen (2001) recommend the use of the solution of Hasan and Kabir (1991). Defining a dimensionless time

$$t_D = \frac{\alpha t}{r_w^2} \tag{3.25}$$

where α is the formation thermal diffusivity and r_w is the wellbore radius. Hence, the function is calculated as

$$f(t) = \begin{cases} 1.1281\sqrt{t_D}\left(1-0.3\sqrt{t_d}\right) & t_D \le 1.5 \\ \left[0.4603+0.5\ln\left(t_D\right)\right]\left(1+\dfrac{0.6}{t_D}\right) & t_D \ge 1.5 \end{cases} \tag{3.26}$$

Calculating the temperature difference between the formation and the inside of the drillstring leads to

$$T_f - T_p = \frac{\dot{q}}{2\pi L}\left(\frac{2}{ID_{dp}h_{dp}} + \frac{\ln\left(OD/ID\right)}{\kappa_{dp}} + \frac{2}{ID_{an}h_{an}} + \frac{\ln\left(OD/ID\right)}{\kappa_{cs}} + \frac{\ln\left(OD/ID\right)}{\kappa_{cm}} + \frac{f(t)}{\kappa_f}\right) \tag{3.27}$$

where the subscripts dp, an, cs, cm and f mean drillpipe, annulus, casing, cement and formation, respectively.

Comparing equations 3.22 and 3.27 it is possible to obtain the Overall Heat Transfer Coefficient as

$$\left(r_{dp}h_o\right)^{-1}=\left(\frac{2}{ID_{dp}h_{dp}}+\frac{\ln\left(OD/ID\right)}{\kappa_{dp}}+\frac{2}{ID_{an}h_{an}}+\frac{\ln\left(OD/ID\right)}{\kappa_{cs}}+\frac{\ln\left(OD/ID\right)}{\kappa_{cm}}+\frac{f\left(t\right)}{\kappa_f}\right) \quad 3.28$$

where h_o is the Overall Heat Transfer Coefficient. The analysis for the heat rate above the mudline is similar.

Ignoring the mechanical energy in the Table 1 and using the same assumptions made for the Momentum Equation, the Energy equation can be written as

$$\rho u\frac{\partial e}{\partial z}=\nabla.q'' \quad 3.29$$

The sink/source term was neglected, since there is no generation of energy inside of the control volume. The divergent term can be treated the same way as it was in the previous section. So the energy equation turns in

$$\rho u\frac{\partial e}{\partial z}=\frac{\pi d}{A}\left(q''_{in}-q''_{out}\right) \quad 3.30$$

where the Heat flux is given by the equation 3.20.

3.3 Equation of State

An Equation of State (EOS) is a function relating thermodynamic state variables (pressure, volume and temperature) of a substance. Most of the equations are empirical or semi-empirical, and cannot be derived mathematically. The most famous EOS is the Ideal Gas Law. The next section will describe the EOS for the density and energy of a drilling fluid.

3.3.1 Density EOS

It is convenient to express EOS for density, ρ, instead of volume, as

$$\rho = \rho(p,T) \tag{3.31}$$

Kaasa et al. (2011) use the concept of bulk modulus, β, and volumetric expansion coefficient, α_v, to present a linearized EOS for density, as equation 3.32. The definitions of bulk modulus and volumetric coefficient of expansion are in equation 3.33 and 3.34 respectively, where the subscription r defines the reference point for the linearization.

$$\rho = \rho_r + \frac{\rho_r}{\beta}(p - p_r) - \rho_r \alpha_v (T - T_r) \tag{3.32}$$

$$\beta = \rho_r \left. \frac{\partial p}{\partial \rho} \right|_T \tag{3.33}$$

$$\alpha_v = -\frac{1}{\rho_r} \left. \frac{\partial \rho}{\partial T} \right|_p \tag{3.34}$$

In general, EOS are developed for pure substance, modification using mixing rules can be made to account for mixtures such as drilling fluids. Hoberock, Thomas and Nickens (1982) presented a compositional model that can be applied to the mixture of oil, water and solids that compose the synthetic drilling fluid. The model is showed below:

$$\rho(p,T) = \frac{\rho_o f_o + \rho_w f_w + \rho_s f_s}{1 + f_o \left(\frac{\rho_o}{\rho_{oi}(p,T)} - 1 \right) + f_w \left(\frac{\rho_w}{\rho_{wi}(p,T)} - 1 \right)} \tag{3.35}$$

where f is the fraction of volume, the subscription o, w and s indicate synthetic oil, brine water and the solids respectively, the subscription i indicates the changes in density due to pressure and temperature. All solids are considered incompressible.

Lima, Barrufet and Juvkam-Wold (1999) created a correlation for the density of the synthetic oil used in Petrobras drilling fluids. The correlation is presented in equation 3.36.

$$\begin{aligned}\rho_{oi} &= p^2\left(-7.4828\times10^{-12}T-1.5261\times10^{-10}\right)+\\ &\quad p\left(1.6937\times10^{-7}T+2.3457\times10^{-5}\right)+\\ &\quad 6.6139-0.00283T\end{aligned} \tag{3.36}$$

McCain (1990) presented a correlation to estimate formation volume factor of brine water as function of pressure and temperature:

$$B_w=\frac{\rho_w}{\rho_{wi}\left(p,T\right)}=\left(1+\Delta V_p\right)\left(1+\Delta V_T\right) \tag{3.37}$$

$$\Delta V_T=-2.2597\times10^{-9}T^3+1.7268\times10^{-6}T^2-5.901\times10^{-5}T \tag{3.38}$$

$$\begin{aligned}\Delta V_p=&-8.977\times10^{-11}p^2-1.2884\times10^{-3}p-3.331\times10^{-13}p^2T\\ &-7.35\times10^{-10}pT-1.8792\times10^{-6}T+0.0013419\end{aligned} \tag{3.39}$$

The combination of equation 3.35 - 3.39 provide an EOS for the density of the synthetic drilling fluids.

3.3.2 Energy EOS

The Equation of State for energy comes from the thermodynamics. The specific heat, c_p, is defined on equation 3.40 and will be used in the study.

$$e=c_pT \tag{3.40}$$

3.4 System of Equation and Boundary Conditions

On this basis, now there is enough background to assembly the system of equation that accurately described the fluid dynamics of the Dual Gradient Drilling.

As proposed by Kaasa et al. (2011) the main assumption is that the drilling fluid can be treated as a viscous fluid. Also, it is assumed a one-dimensional steady state, incompressible flow and neglected the density spatial derivatives, therefore the fluid dynamic is completely described by the following set of equations:

- Balance Equations
  - Continuity (equation 3.4)
  - Momentum (equation 3.18)
  - Energy (equation 3.30)
- Equation of State:
  - Density EOS (Equations 3.35 - 3.39)
  - Energy EOS (Equation 3.40)

The effects of mechanical energy were neglected in the energy equation. As well as the conduction between the walls and the fluid, which implicates they are in thermal equilibrium, and no heat generation will take place.

Therefore, the hydraulic model that describe the fluid dynamics in a drilling system is

$$\begin{aligned} \frac{\partial u}{\partial z} &= 0 && \text{in } \Omega \\ \rho u \frac{\partial u}{\partial z} &= -\frac{\partial p}{\partial z} + 2\frac{f \rho u^2}{d} + \rho g && \text{in } \Omega \\ \rho u c_p \frac{\partial T}{\partial z} &= \frac{2\pi r_o h_o \left(T - T_f\right)}{A} && \text{in } \Omega \end{aligned} \tag{3.41}$$

The PDE's require a set of boundary conditions to close the system. Hence, Essential boundary conditions are applied in the entrance of the domain, $\partial\Omega_g$, meanwhile the Natural boundary condition is applied on the outlet boundary, $\partial\Omega_h$:

$$\begin{aligned} u(0) &= u_o && \text{on } \partial\Omega_g \\ p(L) &= -p_L && \text{on } \partial\Omega_h \\ T(0) &= T_o && \text{on } \partial\Omega_g \end{aligned} \tag{3.42}$$

Solving the continuity equation using velocity boundary condition, it is possible to reduce the system of equation to only two unknown as:

$$\begin{aligned} \frac{\partial p}{\partial z} &= 2\frac{f \rho u_o^2}{d} + \rho g && \text{in } \Omega \\ \rho u_o c_p \frac{\partial T}{\partial z} &= \frac{2\pi r_o h_o \left(T - T_f\right)}{A} && \text{in } \Omega \end{aligned} \tag{3.43}$$

4 FINITE ELEMENT METHOD

The application of the conservation law in Chapter 3 provides a Hydraulic Model based in partial differential equations (PDE). The analytic solution of the system of equation is impossible due the complexity of the system. Therefore, an approximation technique should be used to estimate the values of the variables in the system.

This chapter discusses the Finite Element Method (FEM), applied to the Hydraulic model described above. The first step is to elaborate the Weak Variational Formulation, applying the Method of Weighted Residual.

4.1 Method of Weighted Residual

According to Mennad (1999) a system of equations in the form of 3.43 is called the Strong or Classical formulation because the result of the PDE must be holds for each location at the domain, which sometimes makes the solution unpractical. Hence, a weak variational formulation, which holds only for a specific set of function spaces, should be proposed.

In the Method of Weighted Residual the "strong" system of equations is substituted by a system of residual equation, which is forced to zero in average. The weighted residual consists of the original system multiplied by a weighting function:

$$\int_{\Omega}\left(\mathbf{v}.\mathbf{F}\right)dx=0 \tag{4.1}$$

where $\mathbf{F}$ is the vector with the system's equations, and $\mathbf{v}$ is the weighting or test vector function, each of its component represent the test function of one of the system's equation. The integration is required to guarantee that the residual system satisfy the strong formulation in the average.

Before continuing, it is important to define the function space which the test functions and the approximate solution belongs. The set of function spaces used in the variational formulation are known as Sobolev Spaces, a detailed discussion is presented in Tartar (2007). The most important of the Sobolev Spaces, for this, work are the Lebesgue and Hilbert function spaces, equation 4.2 and 4.3, respectively.

$$L_{p}\left(\Omega\right)=\left\{f\,/\int_{\Omega}\left|f\right|^{p}dx<\infty\right\} \tag{4.2}$$

$$H^{m}\left(\Omega\right)=\left\{f\,/\int_{\Omega}\sum_{\alpha=0}^{m}\left|\frac{\partial^{\alpha}f}{\partial x^{\alpha}}\right|^{2}dx<\infty\right\} \tag{4.3}$$

where $L_{p}\left(\Omega\right)$ is the space of pth-integrable function, meanwhile the $H^{m}\left(\Omega\right)$ is the space of square-integrable functions up to the mth derivative.

Defining the of the test functions spaces as

$$\begin{aligned} R &= H^1(\Omega) \\ W &= L_2(\Omega) \end{aligned} \tag{4.4}$$

where W, and R are the test function spaces for the Momentum and Energy equation, respectively. These spaces should be able to accommodate the essential boundary conditions, then there is a class of subspaces such that

$$\bar{W} = \{v \subset W / v(0) = 0\} \quad \bar{R} = \{v \subset R / v(0) = 0\} \quad \tilde{R} = \{v \subset R / v(0) = T_o\} \tag{4.5}$$

Assuming $v = \{\psi, \varphi\}$ then the variational formulation of the problem resume to find $p, T \in W \times \tilde{R}$ such that

$$\begin{aligned} \int_0^L \psi \frac{\partial p}{\partial z} dx &= \int_0^L \psi \frac{2 f \rho u_o^2}{d} dx + \int_0^L \psi \rho g dx \quad \forall \psi \in \bar{R} \\ \int_0^L \varphi \rho u_o c_p \frac{\partial T}{\partial z} dx &= \int_0^L \varphi \frac{2\pi r_o h_o (T - T_f)}{A} dx \qquad \forall \varphi \in \bar{W} \end{aligned} \tag{4.6}$$

Integrating by parts the pressure gradient term in the Momentum Residual equation:

$$\int_0^L \psi \frac{\partial p}{\partial z} dx = \left(p\psi \big|_{z=L} - p\psi \big|_{z=0} \right) - \int_0^L p \frac{\partial \psi}{\partial z} dx \tag{4.7}$$

as $\psi \in \bar{R}$ the second term in the right-hand side should disappear. So, substituting equation 4.7 in 4.6

$$\begin{aligned} -\int_0^L p\frac{\partial \psi}{\partial z}dx &= \int_0^L \psi \frac{2f\rho u_o^2}{d}dx + \int_0^L \psi\rho g dx - p\psi\big|_{z=L} \quad \forall \psi \in \bar{R} \\ \int_0^L \varphi\rho u_o c_p \frac{\partial T}{\partial z}dx &= \int_0^L \varphi \frac{2\pi r_o h_o \left(T - T_f\right)}{A}dx \quad \forall \varphi \in \bar{W} \end{aligned} \tag{4.8}$$

Introducing the notation $\left(a,b\right) = \int_0^L abdx$, it is possible to rewrite 4.8 as

$$\begin{aligned} -\left(\frac{\partial \psi}{\partial z}, p\right) &= \left(\psi, \frac{2f\rho u^2}{d}\right) + \left(\psi, \rho g\right) - p\psi\big|_{z=L} \quad \forall \psi \in \bar{R} \\ \left(\varphi, \rho u_o A c_p \frac{\partial T}{\partial z}\right) &= \left(\varphi, 2\pi r_o h_o T\right) - \left(\varphi, 2\pi r_o h_o T_f\right) \quad \forall \varphi \in \bar{W} \end{aligned} \tag{4.9}$$

Introducing the by trilinear, bilinear and linear operator:

$$\begin{aligned} b\left(u,v\right) &= \left(u, \frac{\partial v}{\partial z}\right) \\ c\left(u,v\right) &= \left(v, 2\pi r_o h_o u\right) - \left(v, \rho u A c_p \frac{\partial u}{\partial z}\right) \\ f\left(v\right) &= \left(v, \rho g\right) - pv\big|_{z=L} \\ g\left(v\right) &= \left(v, 2\pi r_o h_o T_f\right) \end{aligned} \tag{4.10}$$

Therefore the final form of the Variational Formulation:

$$\begin{aligned} -b\left(p,\psi\right) &= f\left(\psi\right) \quad \forall \psi \in \bar{R} \\ c\left(T,\varphi\right) &= g\left(\varphi\right) \quad \forall \varphi \in \bar{W} \end{aligned} \tag{4.11}$$

4.2 Finite Element Method Approximation

Now that the variational formulation is stated, the next step is to provide approximation from the continuous infinite dimensional space, $\Omega \in \Re^1$, to a finite dimensional discrete space, Ω^h, such that

$$\begin{aligned} \Omega &= \bigcup \Omega^h \\ \partial\Omega_g &\cap \partial\Omega_h = \varnothing \end{aligned} \tag{4.12}$$

where h stands for the length of the each element in the discretization. In this way, there are function subspaces such that $W_h \subset W$ and $\bar{R}_h \subset \bar{R}$. Therefore, the problem resumes to find $p_h, T_h \in W_h \times \tilde{R}_h$ such that

$$\begin{aligned} -b\left(p_h, \psi\right) &= f\left(\psi\right) \quad \forall \psi \in \bar{R}_h \\ c\left(T_h, \varphi\right) &= g\left(\varphi\right) \quad \forall \varphi \in \bar{W}_h \end{aligned} \tag{4.13}$$

where p_h and T_h are the interpolation functions for each finite dimensional space, Ω^h and they are represented as

$$p_h = \sum_{j=1} \varphi_j\left(x\right) c_j^p \quad T_h = \sum_{j=1} \psi_j\left(x\right) c_j^T \tag{4.14}$$

where c_j^p and c_j^T are the nodal degree of freedom associated to the jth node in the element discretization, and ψ_j and φ_j are the trial or shape functions.

The interpolation functions are estimated by polynomials. The temperature polynomials belong to $Q_m\left(\Omega^h\right)$ meanwhile the pressure polynomial belongs to $P_n\left(\Omega^h\right)$, where m and n represent the degree of the polynomial.

Consider $\mathbf{c}=\left\{c_j^p, c_j^T\right\}\in W_h\times\tilde{R}_h$ and $\mathbf{v}=\left\{\mathbf{v_1}, \mathbf{v_2}\right\}$ where $\mathbf{v}_1=\left\{\psi,0\right\}\in\bar{R}_h$, and $\mathbf{v}_2=\left\{0,\varphi\right\}\in\bar{W}_h$. Now defining the new linear forms as:

$$\begin{aligned}\mathbf{K}\left(\mathbf{c},\mathbf{v}\right)&=-b\left(p_h,\mathbf{v_1}\right)+c\left(T_h,\mathbf{v}_2\right)\\ \mathbf{H}\left(\mathbf{v}\right)&=f\left(\mathbf{v_1}\right)+g\left(\mathbf{v_2}\right)\end{aligned} \qquad 4.15$$

The problem turns into: Find $\mathbf{c}\in W_h\times\tilde{R}_h$ such that

$$\mathbf{K}\left(\mathbf{c},\mathbf{v}\right)=\mathbf{H}\left(\mathbf{v}\right)\quad\forall\ \mathbf{v}\in W_h\times\bar{R}_h \qquad 4.16$$

The matrix $\mathbf{K}$ is known as the stiffness matrix of the system and each pair K_{ij} is attached to one variable in a specific node. Therefore, in an elementary point of view, there is a convenient way to order the matrix in which the unknowns are grouped in blocks, as in

$$\mathbf{K}=\begin{bmatrix}K_{pp} & K_{pT}\\ K_{Tp} & K_{TT}\end{bmatrix} \qquad 4.17$$

where the first subscription index indicates the equation related to the unknown variable, while the second indicates the contributions of the unknown to the equation.

Looking at the system of equations, note that all physical components are coupled due to the pressure-temperature dependence in density's equation. However, not all the equations have individual contributions of each unknown, which implicates in void block in the stiffness matrix. Thus, the local matrix assume the form

$$\mathbf{K} = \begin{bmatrix} K_{pp} & 0 \\ 0 & K_{TT} \end{bmatrix} \tag{4.18}$$

Finite Element solution of the Hydraulic Model proposed in the Chapter 3 is obtained by solving the nonlinear system of equations in 4.16. Rannacher (2000) presents different linearization techniques to solve the nonlinear systems, in this work the Newton Method was chosen as the best approach because of it quadratic convergence.

5 DISCUSSION AND RESULTS

The system of equations 4.16 was applied for a RMR configuration and solved using Matlab®. Table 2 shows the input data for the simulation.

The results were tested against the work of Dr. Lima (1999) having excellent agreement, as observer in Figure 5.1.

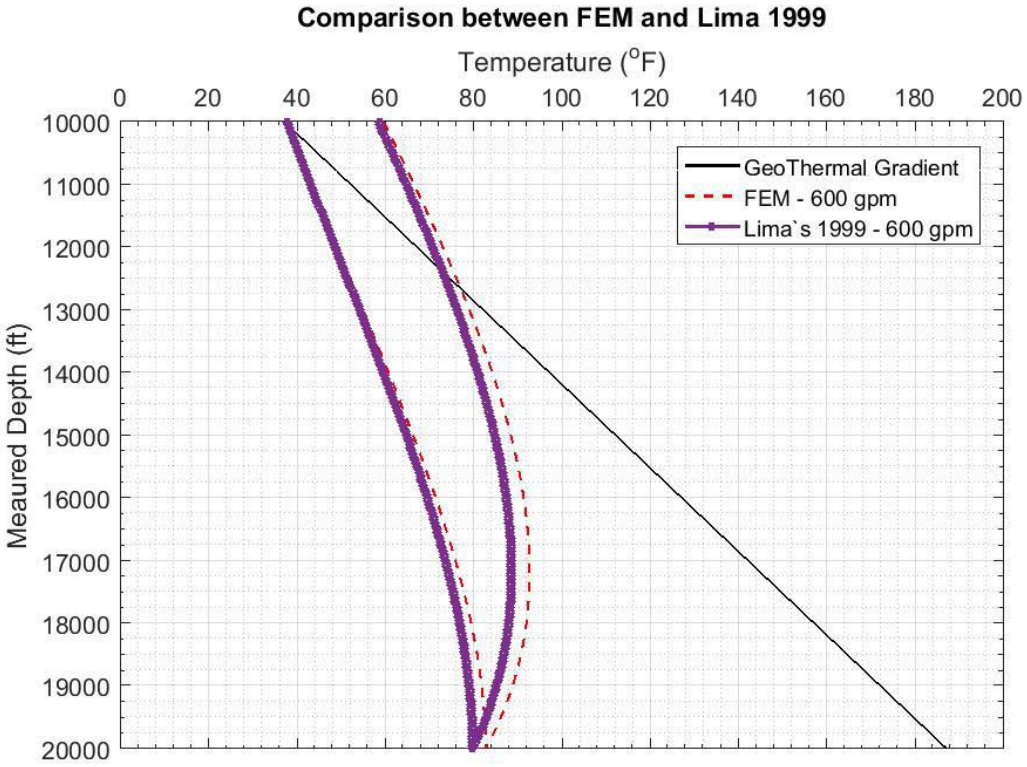

Figure 5.1 – Comparison Between Lima's Results and FEM Technique in the Work.

Table 2 – Input Data for the Simulation using Finite Element Methods.

Flow Rate	600	gpm
Mud Weight	16	ppg
Sea Water Weight	8.6	ppg
Viscosity	46	cp
Yield Point	19	$lbf/100.ft^2$
Water Depth	10,000	ft
Target Depth	20,000	ft
Casing Depth	15,000	ft
Drillpipe OD	5.5	in
Drillpipe ID	4.7	in
Return line OD	6	in
Return line ID	4.5	in
Bit size	8.5	in
Casing ID	9	in
Nozzles	14/32	in
Number of nozzles	3	-
Specific Heat	65	^oF
Drillpipe Heat Transfer Coefficient above mudline	100	$BTU/ht.ft^2.^oF$
Drillpipe Heat Transfer Coefficient above mudline	40	$BTU/ht.ft^2.^oF$
Annular Heat Transfer Coefficient	50	$BTU/ht.ft^2.^oF$
Return line Heat Transfer Coefficient	100	$BTU/ht.ft^2.^oF$
Formation Conductivity	1.4	$BTU/ht.ft.^oF$
Formation Thermal Diffusivity	0.04	ft^2/hr
Geothermal Gradient	1.5	$^oF/100ft$

The effects of flow rate over the Temperature Profile in the drillstring are presented in Figure 5.2. Observe that low flow rates result in higher temperature drop, and the fluid arrives at the mudline almost in thermal balance with the seawater.

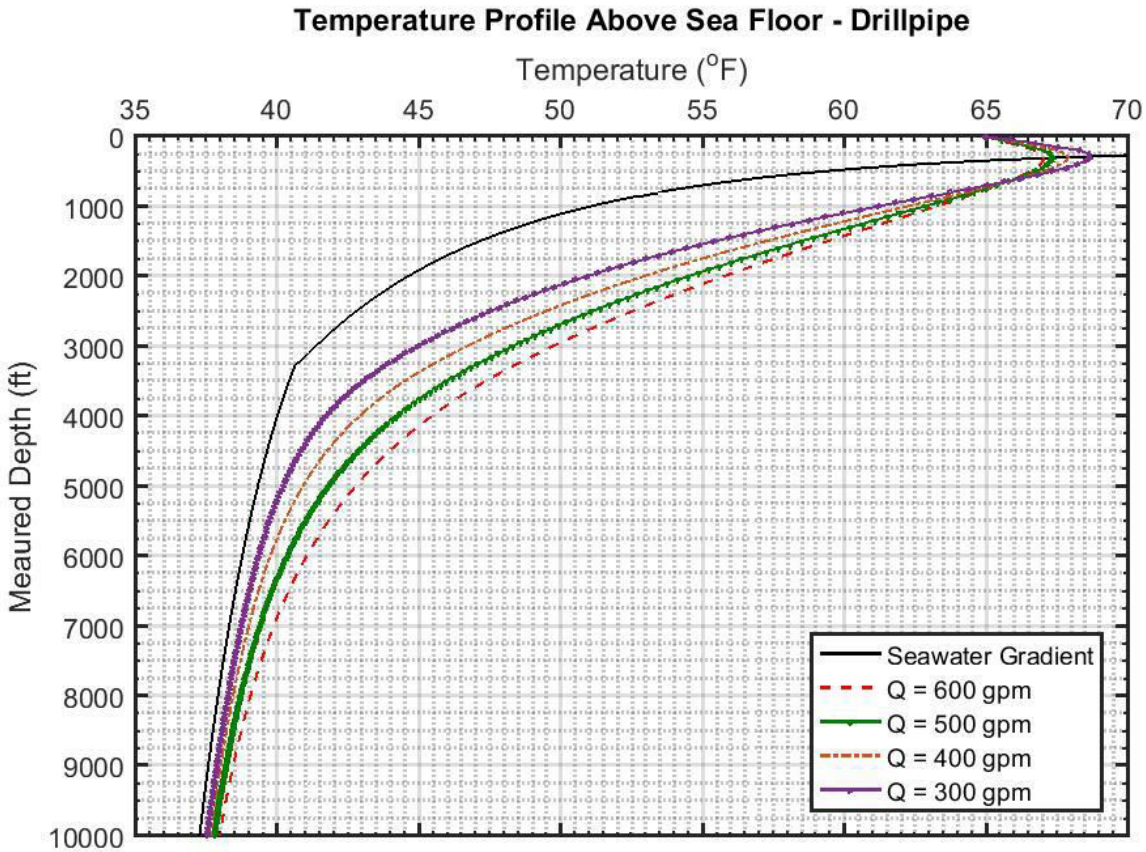

Figure 5.2 – Temperature Profile in Drillstring Above the Mudline, Overall Heat Transfer Coefficient = 100 BTU/ht.ft^2.°F.

Although, the heat rate is highly influenced by the Overall Heat Transfer Coefficient, which is hard to determine in situ, so a sensitivity analysis is presented in Figure 5.3. Note that, at the seafloor level, there is a temperature difference of almost 4ºF between the highest and lowest value of the coefficient, which highlight the importance of proper estimation of this parameter.

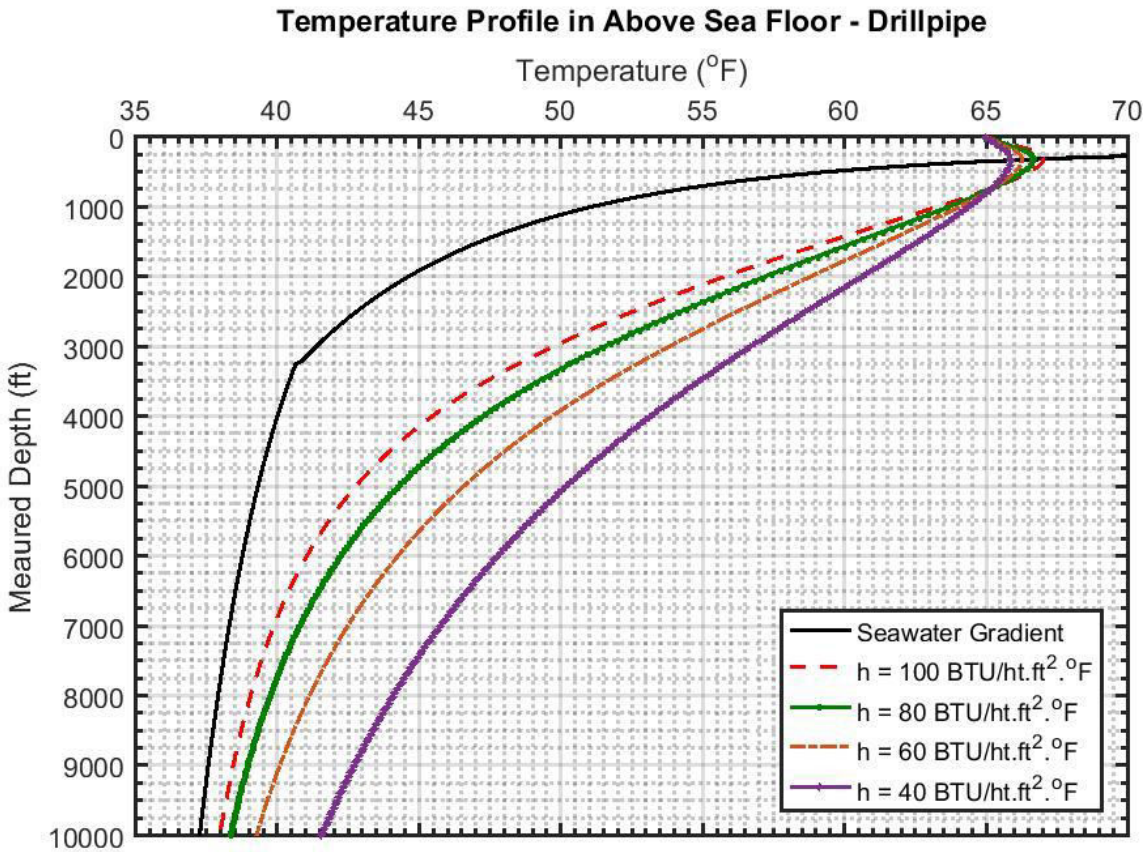

Figure 5.3 – Comparison of the Temperature Drop for Different Values of the Overall Heat Transfer Coefficient, Flow Rate = 600 gpm.

Figure 5.4 shows the Temperature Profile for the Return Line, there is wide variation of temperature in the profile, with inversion of heat flux direction. First, the hot mud leaving the wellbore losses heat to seawater until it reaches the thermal balance. The second, as the fluid keeps moving toward the surface it reaches a region where it is cooler than the seawater, starting to receive heat.

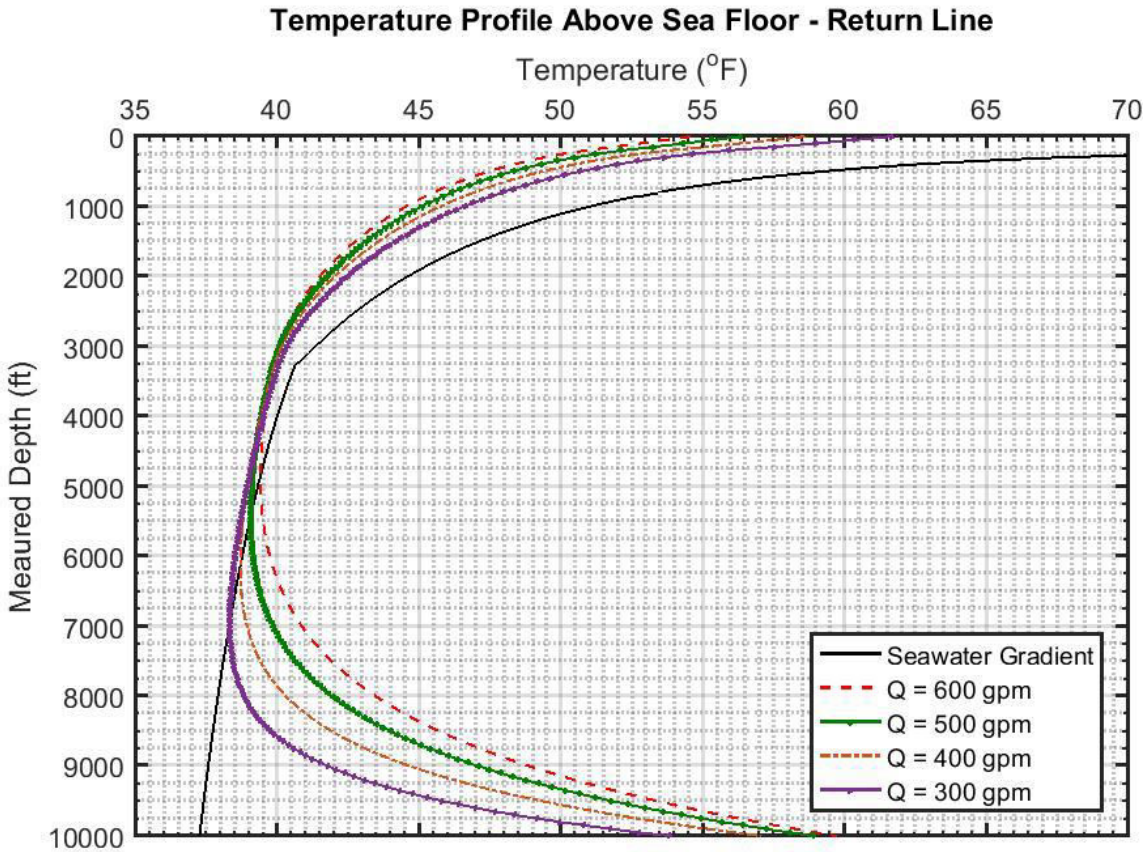

Figure 5.4 – Temperature Profile for Return Line, Overall Heat Transfer Coefficient = 100 BTU/ht.ft^2.°F.

The temperature profile below the mudline relies on the overall heat transfer coefficient, as well as on the geometry of the wellbore. This study considered only the presence of casing, neglecting complex bottomhole assemblies, and the results were consistent with what is presented in the literature, as in Figure 5.1. A sensitivity analysis for two different flow rates is presented in Figure 5.5, even though the effects over the heat rate are similar to those observed above the mudline, it is possible to observe the

effects of the heat exchange between the fluid inside the drillpipe and the fluid in the annular, wherein the annular mud loses heat to the fluid inside the drillpipe.

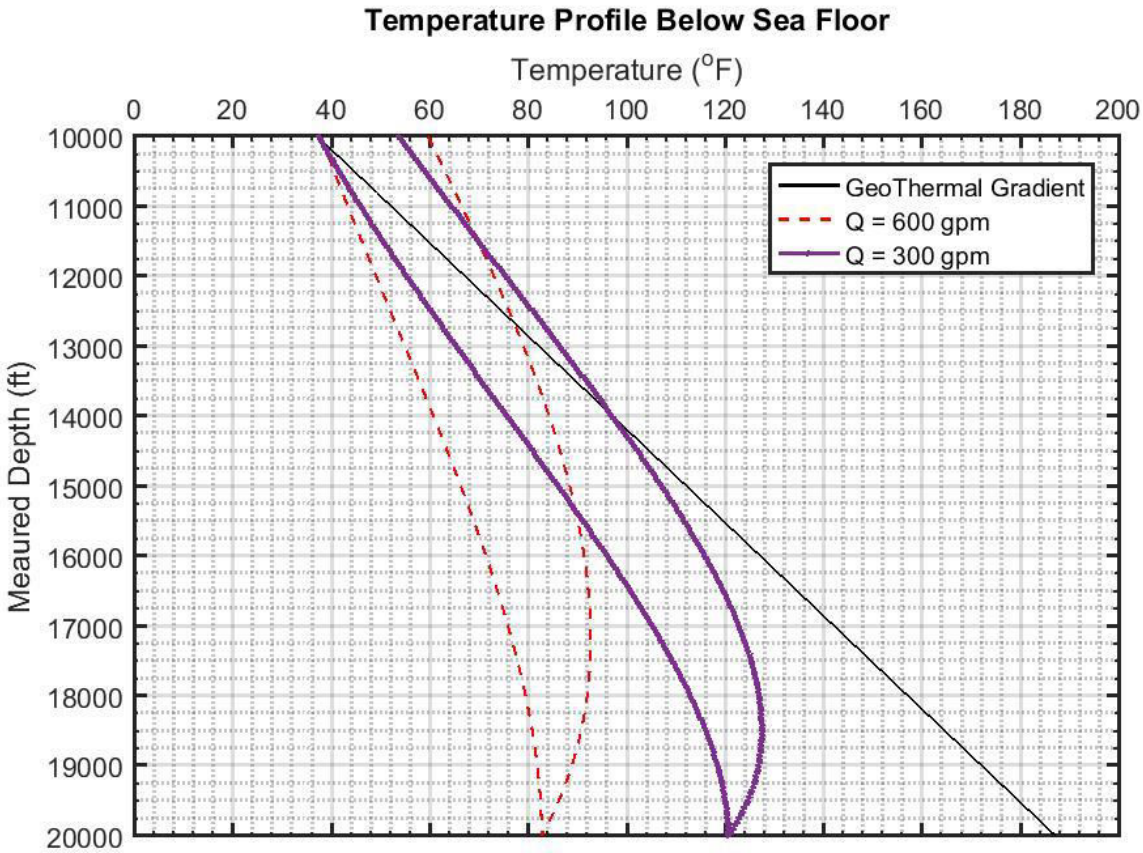

Figure 5.5 – Temperature Profile Below the Mudline.

In the RMR the pressure, at the wellbore head, is keep equal to the hydrostatic pressure at the seafloor, Figure 5.6. Also, observe that the pressure for the flow rate of

300 gpm the stand pipe pressure is practically zero. The annular pressure profile appears to suffer a lot of less influence of the flow rate when compared to the drillstring. This can be explained by the fact the Dr. Lima's mode for the viscosity properties in the annular does not follow a clear trend, and a better model could improve the system.

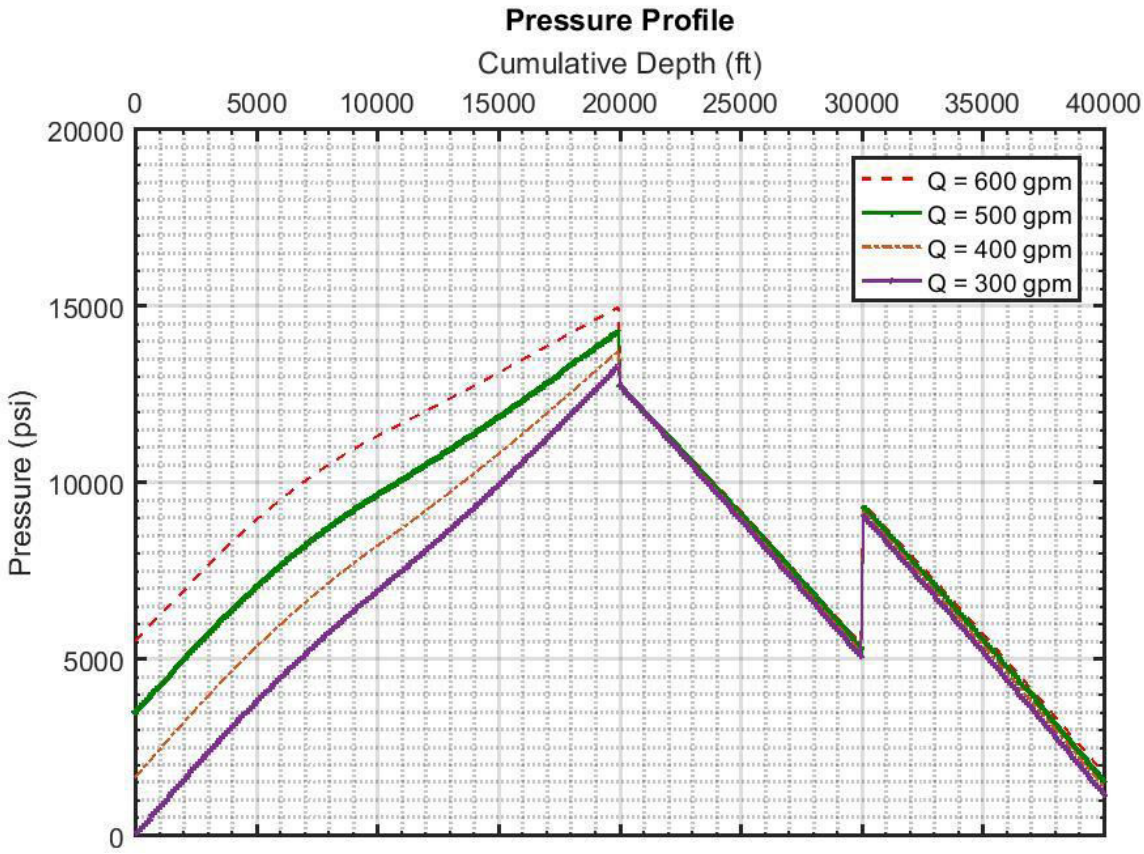

Figure 5.6 – Pressure Profile Along the Fluid Path.

Figure 5.7 illustrates the density profile for different flow rates, observe that a drastic change on density at the bottomhole and at the mudline. These major changes occur because of the big pressure variation at those positions. It is easy to observe when comparing Figure 5.6 and Figure 5.7.

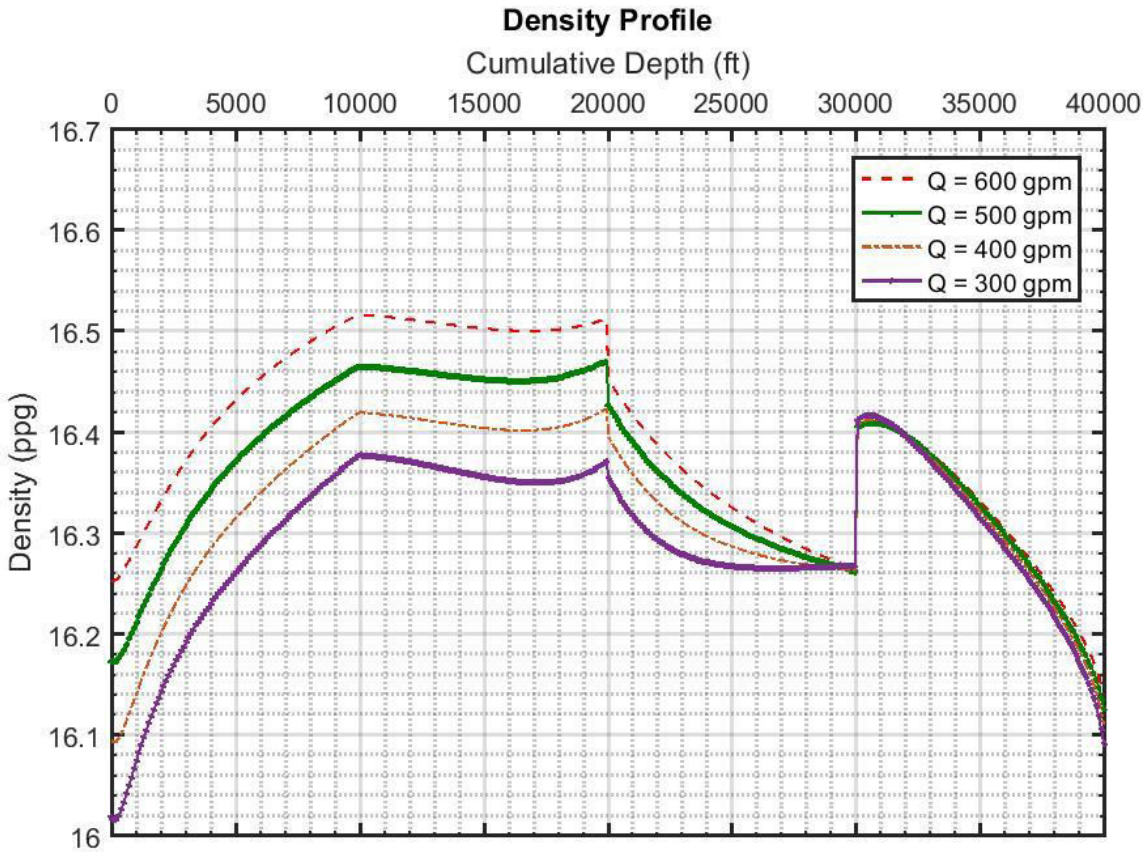

Figure 5.7 – Density Profile Along the Fluid Path, Geothermal Gradient = 1.5 °F/100ft.

6 SUMMARY AND CONCLUSION

As the oil industry has been continuously moving toward the deepwater exploration, the drilling industry has sought for new technologies that can safely overcome the new challenges.

The Managed Pressure Drilling technique, more specifically the Dual Gradient Drilling, could become the standard technique in the next decades, given the intensive effort of the industry to improve and implement it since the middle 90's. However, changing paradigms, in an industry that most of the operations are considered of high risk, could be the biggest barrier to overcome.

The thesis uses the Finite Element Method to solve a Hydraulic Model, based on Lima (1999), that accurately describe the dynamics of the Dual Gradient Drilling.

The model is applicable to most of the drilling scenarios, and in the work it was applied to the Riserless Marine Return System, in order to have a point of comparison with the previous work of Dr. Lima.

The conformation $Q_2 - P_1$ was used to interpolate the approximate solution, and no numerical instabilities were observed. In fact, the results were accurate when compared to the Finite Difference solution in Dr. Lima's work.

The results demonstrated significant changes in the density due the temperature and pressure, highlighting the importance of an accurate density model and its consideration during the development of the well plan.

The sensitivity analysis shows the effects of the Overall Heat Transfer Coefficient over the temperature profile. The results demonstrated that it is the major parameter controlling the heat exchange in the drilling process. However, it is important to notice that the convection was the only mechanism considered in the model, so for a more realistic conclusion, the effects of the conduction in the Overall Heat Transfer Coefficient should be considered. Nevertheless, the estimation of the conductivity of cement and formation are difficult.

In summary, it is possible to conclude that the Finite Element Method provide an accurate solution to the system of PDE in the proposed Hydraulic Model. Also, the density variation can be significant, sometimes exceeding the safe margin.

NOMENCLATURE

Abbreviation:

BHP	Bore Hole Pressure
BOP	Blow out Preventer
DGD	Dual Gradient Drilling
DSV	Drillstring Safety Valve
EOS	Equation of State
FEM	Finite Element Method
JIP	Joint Industry Project
LRRS	Low Riser Return System
MPD	Managed Pressure Drilling
NPT	Non-Productive Times
PDE	Partial differential equations
RMR	Riserless Mud Return
SBM	Synthetic-Based-Mud
SMD	Subsea Mudlift Drilling

Variables and Greek Letters:

A	Cross Sectional Area
B	Formation Volume Factor
d	Diameter
e	Specific Energy
f	Friction Factor
f_i	Fraction of Volume
$f(t)$	van Everdingen-Hurst Flux function
$\mathbf{g}$	Gravity Field
h	Heat Transfer Coefficient
H^m	Hilbert Space
h_o	Overall Heat Transfer Coefficient
$\mathbf{I}$	Identity Matrix
ID	Inner Diameter
K	Flow Consistency Index
L	Length
L_p	Lebesgue Space
n	Flow Behavior Index
$\mathbf{n}$	Outward Normal vector

OD	Outer Diameter
p	Pressure
Q	Generation Rate per unit of Volume
$\dot{q}$	Heat Rate
q''	Heat Flux
r	Radius
R	Temperature Test Space
$\mathbf{T}$	Stress Tensor
T	Temperature
t	Time
$\mathbf{u}$	Velocity Field
W	Pressure Test Space
α	Formation Thermal Diffusivity
α_v	Volumetric Expansion Coefficient
β	Bulk Modulus
$\mathbf{\Gamma}$	Flux Vector
$\dot{\gamma}$	Stain Rate
η	Viscosity
κ	Thermal Conductivity
ρ	Density

$\boldsymbol{\tau}$	Shear Stress Tensor
$\boldsymbol{\tau}_y$	Yield Stress
ψ	Test/Shape Function
φ	Test/Shape Function

Subscripts:

an	Annular
cs	Casing
cm	Cement
D	Dimensionless
h	Discrete space
dp	Drillpipe
f	Formation
o	Oil or Outer
r	Reference Point
s	Solid
w	Water

REFERENCES

API *Recommended Practice 13D*. 2009. Rheology and Hydraulics of Oil-Well Drilling Fluids.25-34. Washington, DC.

Arnold, J.F. 1979. *Riserless Mud Return System*. US4149603 A. USA: Google Patents.

Arrouj, A. 2014. Status on Dual Gradient Technology for Deepwater Drilling. BS in Petroleum Technology Thesis, Norway (May 2014).

Beynet, P.A. 1981. *Drilling Fluid Bypass for Marine Riser*, Company, S.O. USA: Google Patents.

Choe, J. 1995. Dynamic Well Control Simulation Models for Water-Based Muds and Their Computer Applications. PhD in Petroleum Engineering Dissertation, Texas A&M University, College Station, TX (May 1995).

Choe, J. and Juvkam-Wold, H.C. 1997a. Riserless Drilling and Well Control for Deep Water Applications. Presented at the IADC International Deep Water Well Control Conference and Exhibition, Houston, Texas, USA, 15-16 September.

Choe, J. and Juvkam-Wold, H.C. 1997b. Riserless Drilling: Concepts, Applications, Advantages, Disadvantages and Limitations. Presented at the CADE/CAODC Spring Drilling Conference, Calgary, Canada, 8-10 April. CADE/CAODC 97-140.

Choe, J., Schubert, J.J., and Juvkam-Wold, H.C. 2007. Analyses and Procedures for Kick Detection in Subsea Mudlift Drilling. *SPE Drilling & Completion* **22** (04): 7. DOI: http://dx.doi.org/10.2118/87114-PA.

Cohen, J.H. and Deskins, W.G. 2006. Use of Lightweight Solid Additives to Reduce the Weight of Drilling Fluid in the Riser. Presented at the IADC/SPE Drilling Conference, Miami, Florida, 21-23 February. http://dx.doi.org/10.2118/99174-MS.

Crespo, F.E., Ahmed, R.M., and Saasen, A. 2010. Surge and Swab Pressure Predictions for Yield-Power-Law Drilling Fluids. Presented at the SPE Latin American and

Caribbean Petroleum Engineering Conference, , Lima, Peru, 1-3 December. http://dx.doi.org/10.2118/138938-MS.

deBoer, L. 2005. *System and Method for Treating Drilling Mud in Oil and Gas Well Drilling Applications*, Luc, D. Doc. US6926101 B2, pt. USA: Google Patents.

Dowell, J.D. 2010. Deploying the World's First Commercial Dual Gradient Drilling System. Presented at the 2010 SPE Deepwater Drilling and Completions Conference, Galveston, Texas, USA, 5-6 October. SPE-137319-MS. http://dx.doi.org/10.2118/137319-MS.

Eggemeyer, J.C., Akins, M.E., Brainard, R.R. et al. 2001. Subsea Mudlift Drilling: Design and Implementation of a Dual Gradient Drilling System. Presented at the SPE Annual Technical Conference and Exhibition, New Orleans, Louisiana, USA, 30 September-3 October. SPE-71359-MS. http://dx.doi.org/10.2118/71359-MS.

Elieff, B.A.M. 2006. Top Hole Drilling with Dual Gradient Technology to Control Shallow Hazards. MS in Petroleum Engineering Thesis, Texas A&M University, College Station, TX (August 2006).

Falk, K., Fossli, B., Lagerberg, C. et al. 2011. Well Control When Drilling with a Partly-Evacuated Marine Drilling Riser. Presented at the IADC/SPE Managed Pressure Drilling and Underbalanced Operations Conference & Exhibition, Denver, Colorado, 5-6 April. http://dx.doi.org/10.2118/143095-MS.

Fossli, B. and Sangesland, S. 2010. Drilling and Well Control Procedures Using a Partially Evacuated Marine Drilling Riser. Presented at the Well Control Europe, Aberdeen, 13-14 April.

Gaup, T.H. 2012. Simulations of Dual Gradient Drilling: Analytical and Theoretical Studies of Tripping-and Pressure Trapping Operations When Using Dual Gradient Drilling in Deep Waters. MS in Petroleum Engineering Thesis, Gjøvik, Norway (June 2012).

Goldsmith, R. 1998. Mudlift Drilling System Operations. Presented at the Offshore Technology Conference, Houston, TX, 4-7 May. http://dx.doi.org/10.4043/8751-MS.

Gonzalez, R. and Smits, F.S.W. 2002. *Deepwater Drill String Shut-Off*. USA: Google Patents.

Haj, A.M. 2012. Dual Gradient Drilling and Use of Ausmv Scheme for Investiating the Dynamics of the System. MS in Petroleum Technology Thesis, University of Stavenger, Stavanger, Norway (June).

Halkyard, J., Anderson, M.R., and Maurer, W.C. 2014. Hollow Glass Microspheres: An Option for Dual Gradient Drilling and Deep Ocean Mining Lift. Presented at the Offshore Technology Conference-Asia, Kuala Lumpur, Malaysia, 25-28 March. http://dx.doi.org/10.4043/25044-MS.

Hartnett, J.P. and Cho, Y.I. 1998. Non-Newtonian Fluids. In *Handbook of Heat Transfer*, New York: McGraw-Hill.

Hasan, A.R. and Kabir, C.S. 1991. Heat Transfer During Two-Phase Flow in Wellbores; Part I--Formation Temperature. Presented at the SPE Annual Technical Conference and Exhibition, Dallas, TX, 6-9 October. http://dx.doi.org/10.2118/22866-MS.

Hoberock, L.L., Thomas, D.C., and Nickens, H.V. 1982. Here's How Compressibility and Temperature Affect Bottom-Hole Mud Pressure. *Journal Name: Oil Gas J.; (United States); Journal Volume: 80:12* **80** (12): 159-164. DOI:

Howell, J.D., Beck, R.W., Bruce, G.H. et al. 1977. *Drilling Fluid Diverter System*, Company, E.P.R. US 4063602 A. USA: Google Patents.

IADC. 2011. *The UBO & MPD Glossary*. Edtion ed: The Underbalanced Operations & Managed Pressure Drilling Committee of the International Association of Drilling Contractors.

Johansen, T. 2000. Subsea Mudlift Drilling: Evaluation of the Pressure Differential Problem with Subsea Pump. MS in Petroleum Engineering Thesis, Texas A&M University, College Station, TX (August 2000).

Kaasa, G.-O., Stamnes, O., Imsland, L. et al. 2011. Intelligent Estimation of Downhole Pressure Using Simplified Hydraulic Model. Presented at the IADC/SPE Managed Pressure Drilling and Underbalance Operations Conference and

Exhibition, Denver, Colorado, USA, 5-6 April. SPE-143097-MS. http://dx.doi.org/10.2118/143097-MS.

Leach, C.P. 1989. *Method and Apparatus for Deepwater Drilling*, Inc., C. Doc. US4813495 A, pt. USA: Google Patents.

Lima, H.R. 1999. A Dynamic Model of Well Hydraulics in Deepwater Riserless Drilling Operations Using Synthetic-Based Drilling Fluids. PhD in Petroleum Engineering Dissertation, Texas A&M University, College Station, TX (December 1998).

Lima, H.R., Barrufet, M.A., and Juvkam-Wold, H.C. 1999. Pressure Calculations and Kick Detection with Synthetic-Based Muds in a Riserless Drilling Configuration. Presented at the Offshore Technology Conference, Houston, Texas, USA, 3-6 May. OTC-10897-MS. http://dx.doi.org/10.4043/10897-MS.

Malloy, K.P., Stone, R., Medley, G.H. et al. 2009. Managed-Pressure Drilling: What It Is and What It Is Not. Presented at the IADC/SPE Managed Pressure Drilling and Underbalanced Operations Conference & Exhibition, San Antonio, TX, 12-13 February. http://dx.doi.org/10.2118/122281-MS.

Massoud, M. 2005. *Engineering Thermofluids: Thermodynamics, Fluid Mechanics, and Heat Transfer*. New York, NY: Springer Berlin Heidelberg. Original edition. ISBN 9783540272809.

McCain, W.D. 1990. *The Properties of Petroleum Fluids*. Tulsa, PA: PennWell Publishing Co. Original edition. ISBN 0878143351.

Medley, G.H., Jr., Maurer, W.C., and Garkasi, A.Y. 1995. Use of Hollow Glass Spheres for Underbalanced Drilling Fluids. Presented at the SPE Annual Technical Conference and Exhibition, Dallas, TX, 22-25 October. http://dx.doi.org/10.2118/30500-MS.

Mennad, A. 1999. Singular Behaviour of Non-Newtonian Fluids. Master of Technology Thesis, Peninsula Technikon Cape Town

Mewis, J. and Wagner, N.J. 2012. 1. Introduction to Colloid Science and Rheology. In *Colloidal Suspension Rheology*, New York: Cambridge University Press.

Mir Rajabi, M., Toftevag, K.-R., Stave, R. et al. 2012. First Application of Ec-Drill in Ultra Deepwater: Proven Subsea Managed Pressure Drilling Method. Presented at the SPE Deepwater Drilling and Completions Conference, Galveston, Texas, USA, 20-21 June. SPE-151100-MS. http://dx.doi.org/10.2118/151100-MS.

Okafor, U.N. 2007. Evaluation of Liquid Lift Approach to Dual Gradient Drilling. MS in Petroleum Engineering Thesis, Texas A&M University, College Station, TX (December 2007).

Oskarsen, R.T. 2001. Toolkit and Drillstring Valve for Subsea Mudlift Drilling. MS in Petroleum Engineering Thesis, Texas A&M University, College Station, TX (December 2001).

Rannacher, R. 2000. Finite Element Methods for the Incompressible Navier-Stokes Equations. In *Fundamental Directions in Mathematical Fluid Mechanics*, Washington, DC: Springer.

Rehm, B., Schubert, J., Haghshenas, A. et al. 2008. *Managed Pressure Drilling*. Houston, Texas, USA: Gulf Publishing Company. Original edition. ISBN 978-1-399762-24-1.

Schubert, J.J. 1999. Well Control Procedures for Riserless/Mudlift Drilling and Their Integration into a Well Control Training Program. PhD in Petroleum Engineering Dissertation, Texas A&M University, College Station, TX (May 1999).

Schubert, J.J., Juvkam-Wold, H.C., and Choe, J. 2006. Well Control Procedures for Dual Gradient Drilling as Compared to Conventional Riser Drilling. *SPE Journal Paper* **21** (04): 287-295. DOI: http://dx.doi.org/10.2118/99029-PA.

Schumacher, J.P., Dowell, J.D., Ribbeck, L.R. et al. 2001. Subsea Mudlift Drilling: Planning and Preparation for the First Subsea Field Test of a Full-Scale Dual Gradient Drilling System at Green Canyon 136, Gulf of Mexico. Presented at the SPE Annual Technical Conference and Exhibition, New Orleans, Louisiana, USA, 30 September-3 October. SPE-71358-MS. http://dx.doi.org/10.2118/71358-MS.

Seland, S. 1999. Evaluation of Potential Kick Scenarios in Riserless Drilling. MS in Petroleum Engineering Thesis, Texas A&M University, College Station, TX (August 1999).

Sigurjonsson, K.Ö. 2012. Dual Gradient Drilling Simulations. MS in Petroleum Engineering Thesis, Trondheim, Norway (May 2011).

Smith, K.L., Gault, A.D., Witt, D.E. et al. 2001. Subsea Mudlift Drilling Joint Industry Project: Delivering Dual Gradient Drilling Technology to Industry. Presented at the SPE Annual Technical Conference and Exhibition, New Orleans, Louisiana, USA, 30 September-3 October. SPE-71357-MS. http://dx.doi.org/10.2118/71357-MS.

Stave, R. 2014. Implementation of Dual Gradient Drilling. Presented at the Offshore Technology Conference, Houston, TX, 05-08 May. http://dx.doi.org/10.4043/25222-MS.

Stødle, T. 2013. Managed Pressure Drilling from Floaters – Existing Technology & Where Do We Go from Here. MS in Petroleum Engineering Thesis, University of Stavanger, Stavanger,Norway (June 2013).

Tartar, L. 2007. *An Introduction to Sobolev Spaces and Interpolation Spaces*. Pittsburg, PA: Springer Science & Business Media. Original edition. ISBN 3540714839.

Time, A. 2014. Dual Gradient Drilling-Simulations During Connection Operations. MS in Petroleum Engineering Thesis, University of Stavanger, Stavanger, Norway (June 2014).

Tomsic, J.L. 2000. *Dictionary of Materials and Testing* Edtion ed. Warrendale, PA: SAE International.

Vera Vera, L. 2002. Potential Use of Hollow Spheres in Dual Gradient Drilling. MS in Petroleum Engineering Thesis, Texas A&M University, College Station, TX (May 2002).

William, T. 2011. *Dual Gradient Drilling System Using Glass Hollow Spheres*. National Energy Technology Laboratory.

Zhang, Y. 2000. A Hydraulics Simulator for Deep-Water Mud Lift Drilling. MS in Petroleum Engineering Thesis, Texas A&M University, College Station, TX (December 2000).

Ziegler, R., Ashley, P., Malt, R.F. et al. 2013. Successful Application of Deepwater Dual Gradient Drilling. Presented at the IADC/SPE Managed Pressure Drilling and Underbalanced Operations Conference and Exhibition, San Antoni, TX, 17-18 April. http://dx.doi.org/10.2118/164561-MS.

Ziegler, R., Sabri, M.S.A., Idris, M.R.B. et al. 2013. First Successful Commercial Application of Dual Gradient Drilling in Ultra-Deepwater Gom. Presented at the SPE Annual Technical Conference and Exhibition, New Orleans, LO, 30 September-2 Octobe. SPE-166272-MS. http://dx.doi.org/10.2118/166272-MS.